

JINFENG ZHAO

Electrochemical characteristics of Bi(*hkl*) and
micro-mesoporous carbon electrodes in
ionic liquid based electrolytes



DISSERTATIONES CHIMICAE UNIVERSITATIS TARTUENSIS

211

JINFENG ZHAO

Electrochemical characteristics of Bi(*hkl*) and
micro-mesoporous carbon electrodes in
ionic liquid based electrolytes



Institute of Chemistry, Faculty of Science and Technology, University of Tartu,
Estonia

The dissertation is accepted for the commencement of the degree of Doctor of
Philosophy in Chemistry on April 29th, 2022, by the Council of Institute of
Chemistry, University of Tartu.

Supervisors: Prof. Enn Lust,
University of Tartu, Estonia

Research Fellow Ove Oll (PhD),
University of Tartu, Estonia

Opponent: Associate Professor Olivier Crosnier (PhD),
University of Nantes, France

Commencement: 17.06.2022 at 12:15. Auditorium 1020, Ravila 14a, Tartu



European Union
European Regional
Development Fund



Investing
in your future

ISSN 1406-0299

ISBN 978-9949-03-896-1 (print)

ISBN 978-9949-03-897-8 (pdf)

Copyright: Jinfeng Zhao, 2022

University of Tartu Press
www.tyk.ee

CONTENTS

1. LIST OF ORIGINAL PUBLICATIONS	7
2. ABBREVIATIONS AND SYMBOLS	8
3. INTRODUCTION	10
4. LITERATURE OVERVIEW	12
4.1. Ionic liquids	12
4.2. Electrochemistry of electrode ionic liquid interfaces	13
4.3. Energy storage characteristics in supercapacitors	15
4.4. Electrochemical characterization techniques	16
4.4.1. Cyclic voltammetry	16
4.4.2. Constant current technique	17
4.4.3. Electrochemical impedance spectroscopy	18
4.4.4. <i>In-situ</i> scanning tunneling microscopy	19
5. EXPERIMENTAL	23
5.1. Three-electrode electrochemical cell	23
5.1.1. Electrode preparation and cell setup	23
5.1.2. Electrochemical characterizations	24
5.2. Supercapacitor cell	24
5.2.1. Electrode preparation and cell setup	24
5.2.2. Electrochemical characterizations	25
6. RESULTS AND DISCUSSION	26
6.1. Adsorption of anions from ionic liquid at Bi(111) interface	26
6.1.1. Ionic liquid	26
6.1.2. Salt-in-ionic liquid	28
6.1.3. Water-in-ionic liquid	29
6.2. Electrochemical characteristics at Bi(<i>hkl</i>) interfaces	33
6.3. <i>In-situ</i> STM data at Bi(111) and Bi(01 $\bar{1}$) interfaces	36
6.4. Energy storage characteristics of carbon electrode based supercapacitors	39
6.4.1. Perspective of halide ions treated supercapacitors	39
6.4.2. Electrochemical analysis	40
6.5. Outlook: from interfacial structure to energy storage in electrochemical systems	47
7. SUMMARY	51
8. REFERENCES	52
9. SUMMARY IN ESTONIAN	63
10. ACKNOWLEDGEMENTS	65
11. PUBLICATIONS	67

CURRICULUM VITAE	120
ELULOOKIRJELDUS	122

1. LIST OF ORIGINAL PUBLICATIONS

- I O. Oll, M. Väärtnõu, G. Gorbatovski, **J. Zhao**, C. Siimenson, L. Siinor, K. Lust, T. Romann, P. Pikma, E. Lust, Adsorption of anions on bismuth and cadmium single crystal plane electrodes from various solvents and ionic liquid mixtures, *Electrochimica Acta*. 319 (2019) 895–908.
- II **J. Zhao**, G. Gorbatovski, O. Oll, E. Anderson, E. Lust, Influence of water on the electrochemical characteristics and nanostructure of Bi(*hkl*) | ionic liquid interface, *Electrochimica Acta*. 415 (2022) 140263.
- III **J. Zhao**, G. Gorbatovski, O. Oll, T. Thomberg, E. Lust, Effect of alkali and halide ion doping on the energy storage characteristics of ionic liquid based supercapacitors, *Electrochimica Acta*. 319 (2019) 82–87.
- IV **J. Zhao**, G. Gorbatovski, O. Oll, T. Thomberg, E. Lust, Analysis of impedance: the distribution of capacitance in halide ion treated supercapacitors (Under review).

Author's contribution:

- Paper I:** Collaborated in the experimental analysis and data interpretation. Participated in manuscript preparation, editing and formatting.
- Paper II:** Performed all electrochemistry measurements, data analysis and data interpretation. Mainly responsible for the preparation for the manuscript.
- Paper III:** Performed all electrochemistry measurements, data analysis and data interpretation. Mainly responsible for the preparation of the manuscript.
- Paper IV:** Performed all electrochemistry measurements, data analysis and data interpretation. Mainly responsible for the preparation of the manuscript.

2. ABBREVIATIONS AND SYMBOLS

A	electrode area
BF_4^-	tetrafluoroborate anion
BMIm^+	1-butyl-3-methylimidazolium cation
C	capacitance
c	concentration of analyte
CCCD	constant current charge/discharge
CCD	constant current discharge
CDC	carbide derived carbon
C_{dl}	electrical double layer capacitance
C_g	gravimetric capacitance
CPE	constant phase element
C_{pseudo}	pseudocapacitance
C_s	series capacitance at fixed frequency
CV	cyclic voltammetry
CVD	cyclic voltammetry discharge
D	diffusion coefficient
DEME^+	N,N-diethyl-N-methyl-N-(2-methoxyethyl)ammonium cation
E	electrode potential
EC	equivalent circuit
ECSTM	electrochemical scanning tunneling microscopy
EDL	electrical double layer
EDLC	electrical double layer capacitor
EIS	electrochemical impedance spectroscopy
EMImBF_4	1-ethyl-3-methylimidazolium tetrafluoroborate
EMImMeSO_3	1-ethyl-3-methylimidazolium methanesulfonate
EMImOTf	1-ethyl-3-methylimidazolium trifluoromethanesulfonate
EMImTFSI	1-ethyl-3-methylimidazolium bis(trifluoromethylsulfonyl)imide
EMIm^+	1-ethyl-3-methylimidazolium cation
$E_{p,a}$	anodic peak potential
$E_{p,c}$	cathodic peak potential
ΔE_p	difference of peak potentials
$E(t)$	potential at time t
E_0	potential amplitude
F	faraday constant
f	frequency (Hz)
FAP^-	tris(pentafluoroethyl)trifluorophosphate anion
Fc	ferrocene
FSI^-	bis(fluorosulfonyl)imide anion
GCS	Gouy-Chapman-Stern model
h	Planck constant
I	electrode current

i	imaginary number ($\sqrt{-1}$)
IL	ionic liquid
I_p	peak current
$I_{p,a}$	anodic peak current
$I_{p,c}$	cathodic peak current
$I(t)$	current at time t
I_0	current amplitude
J_T	tunneling current
$J_0(V)$	tunneling current amplitude oscillation with applied voltage difference
j	electrode current density
m	mass of an electrode
m_e	electron mass
n	number of electrons
OTf ⁻	trifluoromethanesulfonate anion
PMImI	1-propyl-3-methylimidazolium iodide
PTFE	polytetrafluoroethylene
PYR ₁₃ ⁺	N-methyl-N-propyl-pyrrolidinium cation
PYR ₁₄ ⁺	N-methyl-N-butyl-pyrrolidinium cation
PYR ₁₍₂₀₁₎ ⁺	N-methyl-N-methoxyethyl-pyrrolidinium cation
R	resistance
R_{ads}	adsorption resistance
R_{ct}	charge transfer resistance
R_D	diffusion resistance
R_s	series resistance
RTIL	room temperature ionic liquid
SC	supercapacitor
STM	scanning tunneling microscopy
TFSI ⁻	bis(trifluoromethylsulfonyl)imide anion
t	time
U	cell potential
v	scan rate
Z	impedance
Z'	real part of impedance
Z''	imaginary part of impedance
Z_W	Warburg-like finite-length diffusion impedance
Z_{W-T}	time derived from Warburg element
Z_0	impedance amplitude
Δz	tip-sample distance
ψ^*	average electron emission work function
ω	angular frequency
φ	phase angle shifted
η_{ef}	energy efficiency
σ_s	surface charge density
τ_R	characteristic relaxation time constant

3. INTRODUCTION

In the past decades, the primary interest in interface electrochemistry of ionic liquids (ILs) is due to their unique structure and properties. It includes the adsorption of cations and anions, diffusion of ionic species, kinetics of the electrochemical processes, and electrical double layer (EDL) formation at electrode | IL interfaces, which are the essential subject of electrochemistry in energy storage technologies [1–4]. Variations in the crystallographic structure of the electrode surface, the composition of IL, and the mixtures with IL salts or organic solvents can make considerable differences in the interface structure, observed by the potential dependence of capacitive and resistive behaviour. The electrochemical interface behaviour strongly affects the choice of ILs as electrolytes for the electrochemical power sources.

In this work, the potential dependence of the capacitive and resistive processes at different single crystal bismuth electrodes has been studied in various ILs by cyclic voltammetry (CV), electrochemical impedance spectroscopy (EIS), and *in-situ* scanning tunneling microscopy (STM) methods. The specifically adsorbed anions of ILs and IL salts are the leading cause of the anomalous capacitance maxima in the capacitance vs. potential curves (C , E curves), such as the specific adsorption of Br^- , I^- , and methanesulfonate (MeSO_3^-) anions observed at Bi(111) electrode. In addition, the arrangements of anions from ILs at Bi(111) and Bi(01 $\bar{1}$) planes can be depicted clearly from *in-situ* STM images, which depends on the electrode potentials applied. Interestingly, in the presence of small amounts of water, significant capacitance peaks in the C , E curves are observed in IL 1-ethyl-3-methylimidazolium trifluoromethanesulfonate (EMImOTf) at Bi(hkl) electrodes due to the specific adsorption of OTf^- ions interacted with water molecules. However, there is no capacitance peak in C , E curve for the dried EMImOTf system. Furthermore, because of the effect of water additive, higher capacitance values are obtained at Bi(hkl) | EMImOTf interfaces within the electrode potential region.

Due to the specific adsorption of halide ions from ILs, it is an interesting entry point to increase the capacitance performance of the related electrochemical devices, such as supercapacitors (SCs). Therefore, halide ion and alkali ion salts are adopted in SCs to improve the capacitance performance. The methodology is achieved by the up to 5wt% halide (EMImCl+EMImBr+EMImI) and alkali IL mixtures (LiTFSI+NaTFSI+KTFSI) in 1-ethyl-3-methylimidazolium bis(trifluoromethylsulfonyl)imide (EMImTFSI) soaked into the micro-mesoporous carbon electrodes (halide IL mixture for positive electrode, alkali IL mixture for negative electrode, respectively). Compared with SCs treated with the neat EMImTFSI, the SCs treated with the halide IL mixtures show a remarkable improvement in capacitance performance. However, the SCs treated with the alkali IL mixtures do not show the enhancement of capacitance. Interestingly, the SC treated with the halide (for positive electrode) and alkali (for negative electrode) IL mixtures shows relatively large and highly consistent

capacitance values compared to other SC systems studied. The main reason for improving the capacitance performance is the specific adsorption and redox activity characteristics of both I^- and Br^- ions.

This work aims to provide a fundamental understanding of the electrochemical behaviour of electrode | IL interface from the CVs and C, E curves [I–II]. Another aim of this work is to take advantage of the specifically adsorbed halide ions, which contribute to the capacitance performance of SCs [III–IV]. It demonstrates that a better understanding of the electrochemical interface could give practical guidance for developing novel energy storage devices in the future.

4. LITERATURE OVERVIEW

4.1. Ionic liquids

The ionic liquids (ILs) are liquid salts solely composed of cations and anions below 100 °C, literally defined as room temperature ionic liquids (RTILs) [5–8]. The major attraction for ILs is the extensive possibilities in combinations of cations and anions. That is, the cations and anions can be combined independently in order to optimize the desirable IL types. Most used cations include alkylpyridinium, alkylimidazolium, alkylphosphonium, and alkylammonium cations. The anions are usually BF_4^- , PF_6^- , CF_3SO_3^- , $(\text{CF}_3\text{SO}_2)_2\text{N}^-$, and so forth. According to large numbers of discovered analogous compounds, it is possible to compose 10^6 types of ILs by using different combinations of cations and anions (examples shown in Figure 1) [2]. From the early generation of haloaluminate based ILs to the current non-haloaluminate based ILs, the price of ILs for commercial use has become more and more reasonable and affordable.

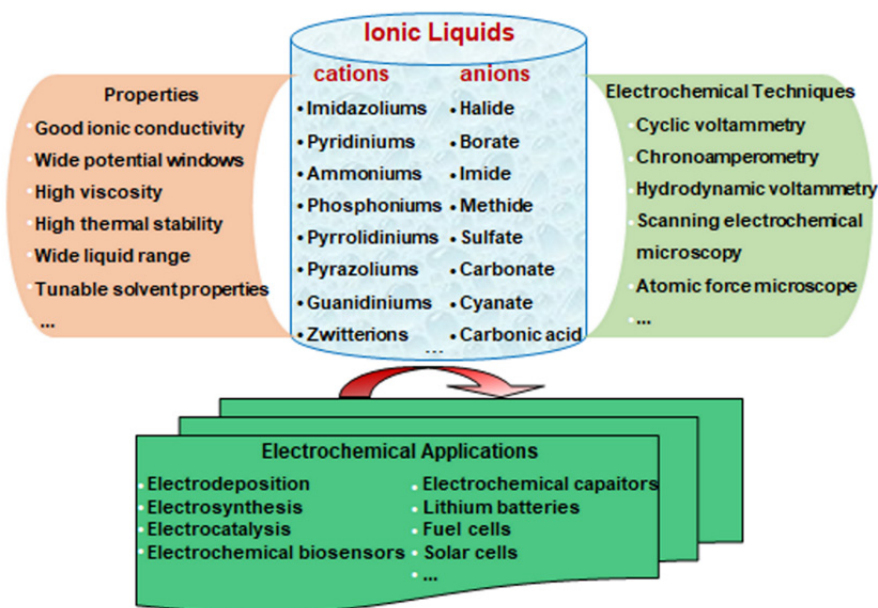


Figure 1. Scheme demonstrating typical ILs, including the properties and electrochemical applications for ILs, and the methods applied to investigate IL electrochemistry [2].

Although the first IL was reported in 1914, half century later, only a few works on ILs were undertaken [9,10]. Nowadays, ILs have gained popularity in the chemistry community due to their excellent physicochemical properties, such as negligible vapor pressure, high electrochemical and thermal stability, and good ionic conductivity [11]. IL applications in green chemistry have drawn much research attention to creating a cleaner and more sustainable chemistry world. One popular application is the electrochemical devices in energy storage and conversion, such as battery technologies, fuel cells, and SCs [3,4,7]. Among these typical applications in electrochemical energy storage devices, ILs are mainly used as electrolyte components. Compared to traditional organic solvent based and aqueous electrolytes, ILs have a unique advantage in the non-flammability and high electrochemical stability to improve electrolyte safety and stability. All these advantages provide more possibilities for IL applications. However, the commercial applications of IL electrolytes are still in their development stage. One possible reason is the prohibitive expense of ILs, especially in comparison with the conventional organic solvent based electrolytes [8]. Despite the recent remarkable progress in the development of ILs, the explorations of more economical and more applicable ILs are still important. Another obstacle is the high viscosity of ILs, which results in relatively low rate capacity, especially for batteries at low temperatures. Thus, the mixtures of ILs and organic solvents have become a popular strategy to decrease the viscosity of electrolytes [12,13].

4.2. Electrochemistry of electrode | ionic liquid interfaces

The fundamental interface electrochemistry of ILs helps to choose a task-specific IL electrolyte because many electrochemical processes involve the adsorption, charge transfer, and diffusion processes of cations and anions, which occur at the interface between electrode and electrolyte. The electrochemical behaviour at the electrode | IL interface has been studied extensively by various techniques, including both computer simulation [14–24] and experimental techniques, for instance, electrochemical impedance spectroscopy (EIS) [25–35], sum frequency generation spectroscopy (SFG) [36,37], atomic force microscopy (AFM) [38–41], and scanning tunneling microscopy (STM) [42–51]. The electrical double layer (EDL) structure is often discussed to understand the electrochemical processes at an electrode | IL interface. The early EDL model describes that EDL behaves like a plane dielectric capacitor, proposed by Helmholtz in 1853 [52]. The Helmholtz model assumes that the counterions stay at the corresponding plate of a capacitor. However, this assumption ignores the space charge of ions behind the layer. Thus, the Helmholtz model cannot explain the minimum value of the differential capacitance curve for diluted solutions. In the early 20th century, Gouy and Chapman proposed the EDL diffusion layer (so-called Gouy-Chapman model) by considering that the counterions in solution form the diffusion layer under the electrostatic force and

thermal motion [53,54]. However, this model assumes the ions as point charges without considering the size of ions, thus neglecting the existence of the compact layer. In 1924, Stern proposed the Gouy-Chapman-Stern model (also known as the GCS model), composed of the Helmholtz compact layer and the Gouy-Chapman diffuse layer [55]. Since the 1940s, many extensions of the GCS model have been given (i.e., the Graham model [56] and Bockris-Devanathan-Müller model [57]).

In an analogy with the classical EDL theory in diluted aqueous solutions and high-temperature molten salts, the EDL structure in ILs should be completely different due to the dual solute-and-solvent properties of ILs. Therefore, there are emerging rediscoveries and modifications in the EDL models of electrode | IL interfaces. The theoretical equation for EDL in IL established by Kornyshev [14] predicted the shape of the differential capacitance curves and the position of the potential of zero charge (pzc) by ignoring the short-range forces between ions and the change of ion volume under polarization. Later, Oldham [58] and Lauw et al. [19] proposed the derivations of the GCS model and concluded the pzc in ILs from the maximum or local minimum capacitance of differential capacitance curves. Afterward, extensive theoretical and modeling studies have been reported [23,24,59–61]. In experimental research, starting from the 21st century, many feature articles on the EDL conceptions and capacitance values at electrode | IL interfaces were published and reviewed [26,47, 62–64]. The Ohsaka group [27,31] systematically studied the interfacial structure at different temperatures by changing the length of alky groups of ILs and electrode types, which primarily described the arrangement of adsorbed cations and anions within EDL obtained from differential capacitance curves. Mao group [48] proposed the diagram-like interface model according to the arrangements of ions at Au(100) | IL interface investigated by STM result.

There is no doubt that the capacitances determined by the EDL characteristics are directly related to the energy storage characteristics of electrochemical devices. More and more data on EDL capacitance in different ILs have been published over the last 20 years, suggesting a significant research prospect. There are several factors that can influence the EDL capacitance in ILs, such as the ion size [19,25,26,61,65–67], electrode material [31,35,65,68], temperature [26–28,64], electrode polarization [26,45], and the interactions both between different ions and between ions and the electrode [61,69,70]. The experimental studies on EDL capacitances have shown the complexity of the electrode | IL interface. For instance, the shapes of differential capacitance curves of the same IL at different electrodes are different. The polarization region of the electrode also affects the ionic structure formed at the interface. The ion arrangements strongly depend on electrode potentials applied, especially at the higher potentials [38]. The specific adsorption of ions causes an increase of EDL capacitance at the typical polarization regime of the electrode. Besides, the capacitances calculated by various methods are somewhat different, suggesting that the available database for EDL capacitance in ILs needs to be further explored.

4.3. Energy storage characteristics in supercapacitors

Capacitance performance is vital for electrochemical devices due to the energy stored within the EDL. Electrochemical capacitors, so-called supercapacitors (SCs), consist of two electrodes, separated by a separator and filled with an electrolyte containing mobile ionic species [71]. Compared with batteries, SC is a short-term energy storage device and delivers high power by one or two mechanisms involving the ions stored/released in EDL and surface faradaic processes [72,73]. One of the strategies for obtaining better performance of SC is to increase the capacity mainly in achieving the maximum of the EDL charging. Therefore, the porosity of carbon electrode materials was optimized [74–78]. Various ILs were tested [79–85]. The pseudocapacitance was obtained using redox active electrolytes [86–89] and pseudocapacitive electrode materials [90–92]. Recently, many efforts have focused on the correlations between the specific surface area and capacitance [74,93,94]. The nanoporous carbide-derived carbon (CDC) electrode materials were optimized to best fit selectively adsorbed ions [74,75,95,96]. Considering the limitation of operating voltages for SCs with conventional solvent-based electrolytes, IL-based electrolytes are promising to allow the realization of high voltage SCs. Some examples are given in Table 1.

Table 1. ILs used as electrolytes for SCs [84].

Ionic liquid	Conductivity [mS/cm]	Viscosity [m Pa s]	ESW [V]	Comments
PYR ₁₄ TFSI	2.2 @ 25°C 6.0 @ 60°C	85 @ 25°C	5.5 @ 60°C	Cycling @ 60°C Voltage: 3–4.0V 25,000 cycles
PYR ₁₍₂₀₁₎ TFSI	3.8 @ RT 8.4 @ 60°C	58 @ 20°C 15 @ 60°C	5.0 @ 60°C	Cycling @ 60°C Voltage: 3–3.8V 25,000 cycles
PYR ₁₃ TFSI	1.4 @ 25°C 4.1 @ 25°C	63 @ 25°C	5.3 @ RT	Cycling @ 60°C Voltage: 3.5V 10% capacitance loss after 800 cycles
PYR ₁₄ FAP	2.2 @ 60°C	292 @ RT	5.6 @ 60°C	Only CVs @ 60°C
PYR ₁₄ OTf	2.0 @ RT 5.5 @ 60°C	n.a.	6.0 @ 60°C	Cycling @ 60°C Voltage: 3.5–3.9V 35% capacitance loss after 20,000 cycles
EMImBF ₄	14 @ 25°C	37 @ 25°C	4.0 @ 25°C	Float voltage 15 days @ 3.0V
EMImTFSI	8.3 @ 25°C	28 @ 25°C	4.1 @ 25°C	Float voltage 2 days @ 3.0V

Ionic liquid	Conductivity [mS/cm]	Viscosity [m Pa s]	ESW [V]	Comments
EMImFSI	15.5 @ 25°C	17.9@ 25°C	4.5 @ 25°C	Self-discharge rate capacity, 10,000 cycles
BMIImBF ₄	3.5 @ 25°C	18 @ 25°C	3.25@ 25°C	CVs, 100cycles
DEMEBF ₄	4.8 @ RT	12 @ RT	6.0 @ RT	500 cycles rate capability

The redox active electrolytes, by adding halide ions [97–100], redox metal ion compounds [87,101,102], and redox molecules [95,103,104], have been deployed to take advantage of the pseudocapacitance effect. A feature example is that an IL mixture of EMImBF₄ and EMImI as an electrolyte can improve the capacitance performance of SCs due to the specific adsorption of iodide ions [98]. However, these redox active components may decrease the maximum cell voltage and accelerate cell degradation of a SC device. This issue can be attributed to the carbon pore blockage with iodide complexes, initiating a significant variation in concentration gradients of electrolytes. The compromise between taking advantage of redox active species and avoiding the pore blockage can be achieved by the proper ratio of different halide ions (I⁻, Br⁻, Cl⁻) to form interhalide compounds [105,106]. Such considerations can provide a possibility for enhancing capacitance without the blockage of pores.

4.4. Electrochemical characterization techniques

4.4.1. Cyclic voltammetry

The cyclic voltammetry (CV) method is used extensively in the electrochemistry community. The working electrode potential (E) is repeatedly scanned from the initial potential to a terminated potential at a specific scan rate and then swept back to the initial potential. The current (I) response to the potential is recorded as an I, E curve, also known as a cyclic voltammogram. CV can give quantitative information on the surface processes.

The characteristic peaks of CVs within the applied potential range show the charge transfer processes at the electrode surface, mainly corresponding to the reduction or oxidation of electrochemically active species. For the reversible electrochemical systems, the peak current, I_p , is simplified by the Randles-Sevcik equation at 298.15 K:

$$I_p = (2.69 \times 10^5) n^{3/2} A c D^{1/2} \nu^{1/2}, \quad (1)$$

where n is the number of electrons transferred, A is the electrode area (cm²), c is the analyte concentration (mol/cm³), D is the diffusion coefficient (cm²/s), and ν

is the scan rate (V/s) [107,108]. Accordingly, the peak current is directly proportional to the concentration. For the mass-transfer controlled processes, the peak current is proportional to the square root of the scan rate.

In addition, there are two parameters derived from CVs: the peak current ratio, $I_{p,a}/I_{p,c}$ (ratio of anodic peak current to cathodic peak current), and the peak potential difference, ΔE_p (potential difference between the anodic peak and the cathodic peak). For a fully reversible redox couple, $I_{p,a}/I_{p,c}$ ($= 1$) strongly depends on the chemical reactions coupled with the redox processes. For a reversible couple, the correlation between the ΔE_p and n is given by equation (2):

$$\Delta E_p = E_{p,a} - E_{p,c} = \frac{0.059}{n} V. \quad (2)$$

For example, a ΔE_p for a fast one-electron process ($n = 1$) is about 59 mV [107,108].

The peak current is controlled by both the charge transfer and mass transfer processes for irreversible and quasi-reversible systems. The ΔE_p value for a one-electron process is not equal to 59 mV. In addition, the individual peaks are reduced in size and widely separated for an irreversible process.

There are no current peaks in the I, E curve for an ideally capacitive system. Therefore, for a symmetrical SC device, the gravimetric capacitance C_g for one electrode can be calculated from the CV data according to the following equation:

$$C_g = \frac{2I}{vm}, \quad (3)$$

where I is the electrode current, v is the potential scan rate, and m is the mass of one electrode.

4.4.2. Constant current technique

The constant current technique is conducted by the current signal as the independent variable to obtain the dependent variable (potential signal) as a function of time. In principle, the instrumentation for the constant current measurement is much simpler than that for constant potential measurement because there is no requirement for feedback from the reference electrode to control the device [107]. Thus, the constant current charge/discharge (CCCD) method is extensively applied in the SCs and battery technologies to describe the performance behaviour, i.e., the energy density and energy efficiency of a device.

For an electrical double layer capacitor (EDLC), the discharge capacitance, $C_{discharge}$, can be calculated from the discharge curve (cell potential (U) vs. time (t) dependence) according to the following equation:

$$C_{discharge} = I \frac{dt}{dU}. \quad (4)$$

To combine with the equation (3), for a symmetrical EDLC device, the discharge capacitance of one electrode can be expressed as

$$C_{discharge} = \frac{2Idt}{dUm}, \quad (5)$$

where, m is the mass of one electrode.

Additionally, the ratio of released energy to stored energy is to evaluate the efficiency of a device, expressed as energy efficiency (η_{ef}). The energy efficiency can also be calculated from the CCCD curves by the integrating area ratio of the discharge curve to charge curve [109]:

$$\eta_{ef} = \frac{\int U(t)dt_{discharge}}{\int U(t)dt_{charge}}. \quad (6)$$

4.4.3. Electrochemical impedance spectroscopy

Electrochemical impedance spectroscopy (EIS) is an effective technique for probing the electrode processes occurring at the electrode | electrolyte interface. The EIS method has become valuable for electrochemically characterizing the power source cells and materials in recent years. The EIS measurements are carried out at different ac frequencies and analyse the response (current or voltage) by applying a small-amplitude perturbation signal (sinusoidal voltage or current) to the electrochemical cell. Then the system response to electrical perturbation (current or potential) is transformed into a new function of impedance (Z) by mathematical calculation. In general, the analysis of the system response gives information about electrode processes and complex interfaces.

Under the EIS measurement, a sinusoidal voltage perturbation is applied to the electrochemical system:

$$E(t) = E_0 \sin \omega t, \quad (7)$$

where $E(t)$ is the potential at time t , E_0 is the potential amplitude, ω is the angular frequency (rad s^{-1}) with relation to frequency f (Hz): $\omega = 2\pi f$. The current response $I(t)$ to the voltage perturbation at the same frequency is given by

$$I(t) = I_0 \sin \omega t + \varphi, \quad (8)$$

where $I(t)$ is the current at time t , I_0 is the current amplitude, and φ is the phase shifted between voltage and current sinusoidal wave. According to Ohm's law, the impedance (complex resistance), Z , is expressed by

$$Z = \frac{E(t)}{I(t)}. \quad (9)$$

Obviously, the impedance is a vector quantity. Impedance can be simply expressed by using the complex notation:

$$Z = Z_0(\cos \varphi + i \sin \varphi) = Z' + iZ'', \quad (10)$$

where the impedance Z_0 has the unit of resistance with a magnitude $Z_0 = E_0/I_0$, Z' is the real part of impedance, Z'' is the imaginary part of the impedance, and $i = \sqrt{-1}$ [107,110,111].

The ultimate purpose of EIS measurement is to determine the contribution of the double layer, electron transfer, mass transfer processes to an electrochemical system. The EIS technique is a transient record based on the voltage or current response, which describes the electrode processes in electrochemical systems. The resulting impedance spectrum, known as the Nyquist plot, contains extensive information about the electrified interface and electron transfer process. Based on a circuit concept in electrical engineering practice, an electrochemical system is generally described by resistive, charge transfer, diffusion, and capacitive behaviour. In the case of a combination of resistance and capacitance, the real part Z' and imaginary part Z'' of an impedance complex plane show the resistive and capacitive characteristics of an electrochemical system, respectively. Therefore, an equivalent circuit (EC) containing simple physical elements has been applied to calculate the impedance data.

As an EC element, a pure resistor is fully resistive with $Z_0 = R$ and $\varphi = 0$ at any frequencies. Additionally, a pure capacitor can behave fully capacitive ($\varphi = -90^\circ$), and corresponding frequency-dependent capacitance C can be calculated from $Z_0 = \frac{1}{\omega C} = \frac{1}{2\pi f C}$.

In general, an EC consisting of both resistor and capacitor elements can describe the processes that take place at electrochemical interfaces. However, the EC model has many extensions for analysing the interface characteristics between electrolyte and electrode. For example, the constant phase element (CPE) describes the EDL capacitance to eliminate the experimentally observed capacitance dispersion effect [26,28,31,62]. Besides, the most suitable EC scheme should fit well with the experimental impedance data and have a valid physical meaning for interfacial processes.

4.4.4. *In-situ* scanning tunneling microscopy

Over the last two decades, the scanning tunneling microscopy (STM) technique has been widely used to analyse surface structure at the atomic resolution level, commonly for well-defined and atomically smooth surfaces. Among the probe microscopes family, the STM was early developed by Gerd Binnig and Heinrich Rohrer in 1981 [112]. The critical principle of STM is that the tunneling current (J_T) flows through a narrow potential barrier between the conducting sample surface and a sharp metal tip when the tip approaches close to the surface, i.e., less than a few nanometres. Electron tunneling occurs under the over-

lap of wave functions between the tip and sample surface atoms. According to the quantum mechanics theory and extensions applied, J_T can be expressed approximately by a simple formula [113]:

$$J_T = J_0(V)e^{-\frac{4\pi}{h}\sqrt{2m_e\psi^*}\Delta z}. \quad (11)$$

As the equation shows, the tunneling current depends exponentially on the tip-sample distance, Δz . The exponential dependence of tunneling current on the distance between the tip and surface atoms provides the sensitivity of measured current, which allows obtaining high spatial resolution of surface structure [114,115]. In addition, other factors also influence the tunneling current, the value $J_0(V)$, which is assumed to be independent of the tip-sample distance, the average electron emission work function ψ^* , electron mass m_e , and Planck constant h ($6.62607015 \times 10^{-34} \text{J} \cdot \text{Hz}^{-1}$).

Generally, there are two measurement modes to obtain the STM image. One is the constant current mode. The tip scans over the surface at a constant current by continuously tuning the vertical position of the tip under a feedback mechanism. Another is the constant height mode. The tip moves above the surface at a constant distance of several angstroms to record the changes in tunneling current. It is more effective to investigate an atomically smooth surface in this mode. This mode allows investigating the real-time changes occurring on a surface by applying very high scan rates and a quick record of STM images [115].

An extension, electrochemical STM (ECSTM), also known as *in-situ* STM (to observe the real-time changes occurring on the surface), combines basic STM and classical electrochemical methods. The *in-situ* STM measurement can give valuable information on the structure of electrode | electrolyte interface, the dynamic of the surface process, and the formation of an electrochemical new phase at a nanoscale. Although the fundamentals of *in-situ* STM are the same as conventional STM, additional notes for *in-situ* STM are the three-electrode electrochemical cell where the sample substrate is used as a working electrode and the development of suitable probes to image the surface morphology under potential control. In the bipotentiostat approach, both tip and sample electrode potential are independently controlled by referring to a reference electrode in liquid environments. A corresponding bipotentiostat configuration is given in Figure 2 [115]. In this configuration, the potentiostats control the potentials of the tip and working electrode substrate separately with regard to the reference electrode.

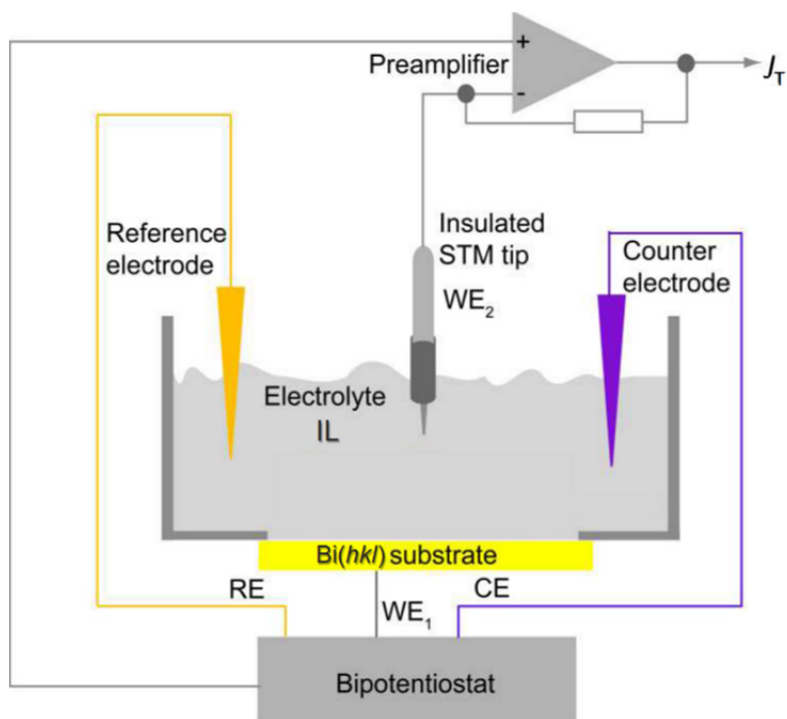


Figure 2. *In-situ* STM configuration, bipotentiostat approach to control the potentials of both tip and sample electrode [115].

In principle, for ECSTM, the current flowing through the tip includes three components: (1) STM tunneling current, (2) capacitive current by the charge-discharge process within the EDL regime at the tip | electrolyte interface, and (3) faradaic current caused by the electrochemical reaction at the tip surface (if there is a faradaic reaction) [115]. The STM measurement can be interfered by the latter two currents, (2) and (3), even worse if these two types of currents are higher than the STM tunneling current itself. In this case, these two electrochemical contributions should be suppressed to make the STM measurement available under the tip current being considerably more prominent than the electrochemical currents. Except for individually minimizing the electrochemical currents, another practical approach is the tip coated by an electric insulator to reduce the faradaic and capacitive currents. The coating materials for tip insulation should be chemically stable in an electrolyte solution. Commonly used coating materials are ApiezonTM wax, organic polymers, and glass [116]. In addition, the STM tips are commonly prepared by the electrochemically etched tungsten wire, meanwhile keeping the tip apex uncoated.

As mentioned above, the current flowing through the tip can be very sensitive to different stages so that *in-situ* STM measurements are not that easily exercisable. The *in-situ* STM result for an electrochemical interface is also related to

the sample preparations, including the atomically flat substrate, highly clean substrate, a well conductive substrate, and a considerably stable surface [117, 118]. Many surface treatment methods have been applied to prepare electrodes for STM measurements, such as the electrochemical polishing [119,120] and mechanical cleaving [45] procedures used for Bi electrodes. These stringent requirements of the *in-situ* STM technique are essential in providing detailed surface structure information at an atomic level in electrochemical interface studies. On the other hand, surface studies by *in-situ* STM have witnessed significant success in obtaining STM images of atomic scale under electrochemical processes. One example is the potential-dependent surface structure at the electrode | electrolyte interface [121–124].

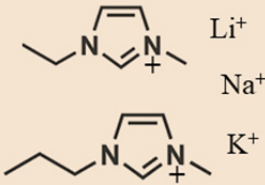
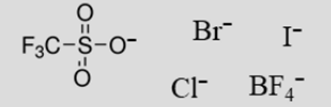
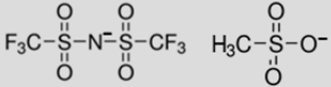
5. EXPERIMENTAL

5.1. Three-electrode electrochemical cell

5.1.1. Electrode preparation and cell setup

Ionic liquids, 1-ethyl-3-methylimidazolium trifluoromethanesulfonate (EMImOTf, 99.5%, Solvionic), 1-ethyl-3-methylimidazolium bis(trifluoromethylsulfonyl)imide (EMImTFSI, 99.5%, Solvionic), 1-ethyl-3-methylimidazolium tetrafluoroborate (EMImBF₄, 99%, Solvionic), 1-ethyl-3-methylimidazolium methanesulfonate (EMImMeSO₃, 99.5%, Solvionic), 1-ethyl-3-methylimidazolium bromide (EMImBr, 99.9%, Io-Li-Tec), and 1-propyl-3-methylimidazolium iodide (PMImI, 99.9%, Merck), were applied as electrolytes in three-electrode electrochemical cell systems (the components of ILs are shown in table 2). The drying procedure for ILs was carried out in an ultrahigh vacuum at 70 °C for 72 hours. The water content of neat EMImOTf is less than 20 ppm provided by the Karl-Fisher analysis report. A uniform diluted solution of 0.1 wt% H₂O in EMImOTf was prepared [125]. The working electrodes, Bi(111), Bi(01 $\bar{1}$), and Bi(001), were first mechanically polished with sandpaper and then electrochemically polished in KI and HCl aqueous solution. The counter electrode (Pt net) and reference electrode (Pt wire) were prepared with flame annealing and ultrapure water rinsing. The reference electrode was immersed in a Luggin capillary filled with test IL to separate it from the working electrode. The reference electrode potential was calibrated in EMImBF₄ containing a moderate amount of ferrocene (Fc, 98%, Sigma-Aldrich). The calibration procedure was conducted in a three-electrode electrochemical cell. The Pt wire was used as a working electrode, Pt net as a counter electrode, and Pt wire in a Luggin capillary filled with EMImBF₄ as a reference electrode [70]. The prepared ILs and IL mixtures, bismuth single crystal electrodes, Pt net, and Pt wire were assembled into a three-electrode electrochemical cell inside an Ar-filled glove-box (H₂O < 1 ppm, O₂ < 1 ppm).

Table 2. The anions and cations of ILs studied in this work.

Cations	Anions
 Li ⁺ Na ⁺ K ⁺	 F ₃ C-SO ₂ O ⁻ Br ⁻ I ⁻ Cl ⁻ BF ₄ ⁻
	 F ₃ C-SO ₂ -N-SO ₂ -CF ₃ H ₃ C-SO ₃ O ⁻

5.1.2. Electrochemical characterizations

The assembled three-electrode cell systems were investigated and characterized by CV, EIS (Autolab PGSTAT 320 with FRA II), and *in-situ* STM (Agilent Technologies 5500 and Molecular Imaging MS300) techniques. The CV measurement was done at the potential scan rate of 1–100 mV/s. The EIS measurement was conducted at the frequency range from 10^4 to 10^{-1} Hz with 15 mV perturbation amplitude. The tungsten wire (diameter 0.25 mm, purity 99.9%, Jülich, Mateck) as the STM tip was electrochemically etched in a KOH (Sigma-Aldrich, puriss) aqueous solution. The STM data were analysed by Gwyddion software [126].

5.2. Supercapacitor cell

5.2.1. Electrode preparation and cell setup

The carbon electrode material with the micro-mesoporous structure was prepared from SiC-CDC material synthesized from SiC powder by gas-phase chlorination at 1100 °C and followed by CO₂ activation at 950 °C [82,127]. Then the SiC-CDC powders were mixed with 5wt% of binder (polytetrafluoroethylene, PTFE, 60% dispersion in H₂O, Sigma-Aldrich), laminated, and roll-pressed several times (Nippon Kodoshi) to prepare the carbon sheet with the thickness of $100 \pm 5 \mu\text{m}$. After drying under vacuum, a pure Al layer was deposited on one side of the carbon sheet and then cut into a round carbon electrode with the geometric surface area of 2 cm² and the average mass of 17 ± 3 mg [128].

The mixtures for treating the positive electrode were prepared by mixing EMImTFSI with up to 5 wt% of halide salt mixtures by a certain mole ratio, EMImCl (98%, Merck KGaA) : EMImBr (99%, IoLiTec) : EMImI (99%, Merck KGaA) = 1:4:2. The mixtures for treating the negative electrode were prepared by mixing EMImTFSI with up to 5wt% of alkali salt mixtures by a certain mole ratio, LiTFSI (99.9%, Solvionic): NaTFSI (99.5%, Solvionic): KTFSI (99.5%, Solvionic) = 1: 1: 1. The order of oxidation of halide ions was considered when determining the ratios of each additive [128]. The electrodes were soaked in the IL salt mixtures for overnight under vacuum and then treated by removing the excess liquid. The separator sheet was soaked by neat EMImTFSI. For a blank comparison, both positive and negative electrodes were treated in EMImTFSI. The soaked positive and negative electrodes and a separator sheet were assembled in a standard two-electrode Al test cell (HS Test Cell, Hohsen Corporation) in an Ar-filled glovebox (H₂O < 0.1 ppm, O₂ < 0.1 ppm). All SC cells were filled with EMImTFSI as electrolytes.

5.2.2. Electrochemical characterizations

The electrochemical characterizations of assembled SC cells were by the CV, CCCD, and EIS methods, using the SI1287 Solartron potentiostat with a 1252A frequency response analyzer via ac frequency (f) range from 300 kHz to 1 mHz at 5 mV perturbation amplitude. All electrochemical experiments were carried out at room temperature of 22 ± 1 °C.

6. RESULTS AND DISCUSSION

6.1. Adsorption of anions from ionic liquid at Bi(111) interface

6.1.1. Ionic liquid

The electrochemical interface behaviour for Bi(111) electrodes in different ILs is shown in Figure 3a, the dependence of series capacitance (C_s) on electrode potential (E) at 10 Hz, namely the C_s , E curves. The detailed calculations of C_s values are based on the imaginary part of the impedance complex plane. The potential regions of C_s , E curves are determined by the CVs that show the ideally polarizable potential region [129]. The whole potential region of C_s , E curves includes two potential ranges: one is the most negative potential range (from -2.2 V to -1.9 V vs. Fc/Fc^+), indicating a high similarity for studied ILs. Another is the less negative potential region (from -1.9 V to positive potential end), showing the significant discrepancies between ILs. For the $\text{Bi}(111) | \text{PMImI}$ system, the C_s values start increasing significantly at above -1.6 V, explained by the specific adsorption of I^- ions, namely the strong interaction between I^- ions and Bi(111) electrode within the first interfacial layer [70]. Accordingly, for the $\text{Bi}(111) | \text{EMImMeSO}_3$ system, the C_s values start increasing at above -1.9 V, associated with the specific adsorption of MeSO_3^- ions at charged Bi(111) electrode. While, relatively low C_s values are observed in EMImOTf , EMImTFSI , and EMImBF_4 within the less negative potential region, suggesting that the difference in C_s values at this range mainly corresponds to the volumes of each anion.

Interestingly, the specifically adsorbed I^- ions at Bi single crystal electrodes contribute to the enhancement of capacitance in neat IL, I^- ions contained aqueous solutions, and organic solvent solutions [130–132]. In addition, the C_s , E curves with both scanning directions show that the adsorption-desorption process of I^- ions from PMImI is highly reversible [129,132]. It suggests that a unique contribution of halide anions could help increase the C_s values within the ideal polarization region, which directly relates to the SC charge storage capacity. Examples of high-performance SCs in the presence of iodide ions have been reported [89,97,100,133].

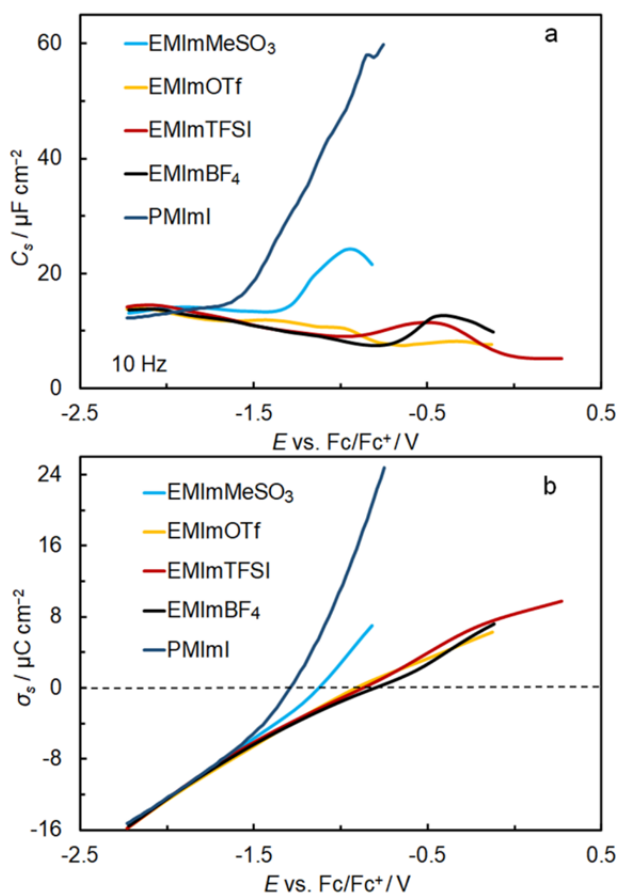


Figure 3. Series capacitance (C_s) vs. electrode potential (E) curves at 10 Hz (a) and surface charge density (σ_s) vs. electrode potential (E) curves (b) for Bi(111) | IL interfaces.

In terms of the ions adsorption process within EDL, the surface charge density (σ_s) of specifically adsorbed ions from ILs has been calculated according to the Hurwits-Parsons-Dutkiewicz method [134,135], providing the adsorption characteristics.

Figure 3b presents the σ_s , E curves for Bi(111) electrodes in different ILs. The σ_s , E curves for EMImBF₄, EMImOTf, and EMImTFSI are highly consistent within the negative potential region, explained by the surface-inactive nature of cations. Similar to the response of C_s , E curves, the σ_s , E curves for EMImMeSO₃ and PMImI show a significant change in σ_s within the less negative potential region, as the surface-active anions, both MeSO₃⁻ and I⁻ have a specific interaction with the bismuth electrode. Thus, the specific adsorption of anions on electrodes is mainly controlled by their activity and specific structures.

6.1.2. Salt-in-ionic liquid

As depicted above, the specifically adsorbed halide anions from ILs contribute to increasing capacitance. Generally, the ILs composed of halide anions (i.e., I^- , Br^- , Cl^-) are solid-state at room temperature. Taking the consideration that halide ions contained IL salts can be dissolved in organic solvents [136–139] and ILs [69,140–142], the adsorption of halide ions from these non-aqueous electrolytes at Bi single crystal electrodes has been studied systematically, including the different concentrations in ILs [129,140,142,143]. However, the adsorption of halide ions is a complex process, which contributes to the different interfacial structures formed. Figure 4 shows the influence of bromide ion concentration in IL.

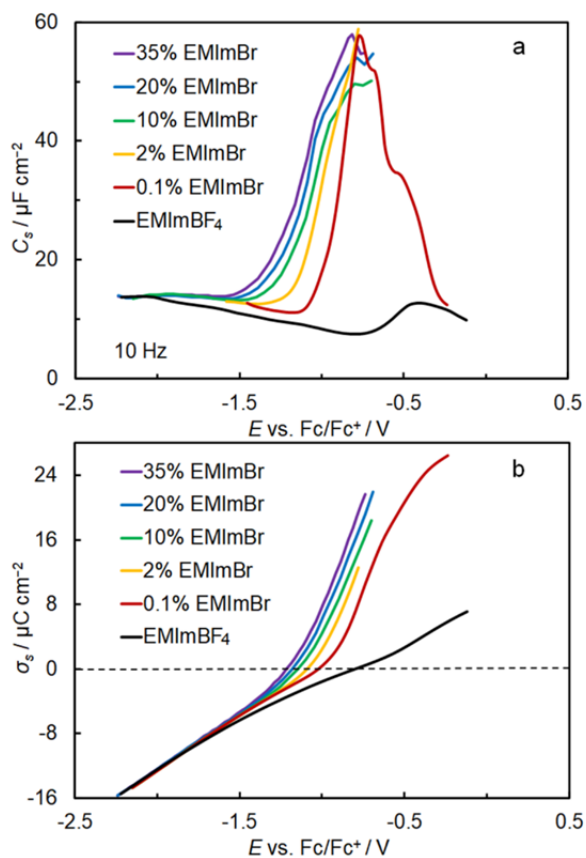


Figure 4. Series capacitance (C_s) vs. electrode potential (E) curves at 10 Hz (a) and surface charge density (σ_s) vs. electrode potential (E) curves (b) for Bi(111) electrode in EMImBF $_4$ and EMImBF $_4$ + X%EMImBr mixtures.

Figure 4a shows the C_s , E curves for EMImBF₄ and its mixture with EMImBr at 10 Hz. C_s values are around 7~14 $\mu\text{F cm}^{-2}$ for EMImBF₄ within the studied potential range. Compared to the EMImBF₄, the C_s , E curves for the mixtures of EMImBr in EMImBF₄ show the characteristic capacitance maxima up to 58 $\mu\text{F cm}^{-2}$ due to the specific adsorption of bromide ions. Interestingly, the C_s values preferably begin to increase at more negative potentials when the EMImBr concentrations increase, suggesting that the adsorption bond between the Bi(111) surface and the bromide ions becomes strong under the high EMImBr concentrations.

A similar trend on the σ_s , E curves are shown in Figure 4b. Due to the specific adsorption of bromide ions from IL mixtures, the σ_s values increase rapidly when $E > -1.5$ V. This increase is related to the concentration of Br⁻ ions in IL mixtures. However, when $E < -1.5$ V, there is no noticeable difference in neither neat EMImBF₄ nor EMImBr salt mixtures, as shown in Figure 4. This phenomenon can be explained by the surface-inactive EMIm⁺ cations predominantly adsorbing on the most negatively polarized Bi(111) electrode. When $E > -1.5$ V, the Br⁻ ions begin to adsorb on the surface, which depends on the activity and concentration of adsorbed ions themselves at the Bi(111) electrode.

6.1.3. Water-in-ionic liquid

Although the increased capacitance has been observed in the Br⁻ and I⁻ contained ILs, the presence of halide ions narrows the potential range of electrochemical stability of the system [129,140,141] as the electrolyte itself becomes somewhat more reactive to cause faradaic processes. Besides, the addition of halide IL salts can introduce small amounts of water, which can somehow reduce the electrochemically stable potential range of electrolytes.

Small amounts of impurities remaining in the ILs during the manufacturing process, such as traces of water and halide ions, cannot be avoided. However, such impurities can limit the electrochemically stable potential region for IL electrolytes. In the case of hydrophilic IL, the absorption of water from the atmosphere cannot be removed entirely in laboratory systems and practical applications. Interestingly, in respect of the high viscosity of IL, small amounts of water in ILs may somewhat reduce the base viscosity. It is of great importance to demonstrate how water molecules behave and affect the structure of the electrode | IL interface. The main objective of this part is to systematically investigate the electrochemical behaviour of Bi single crystal electrodes in hydrophilic EMImOTf (with and without small amounts of water).

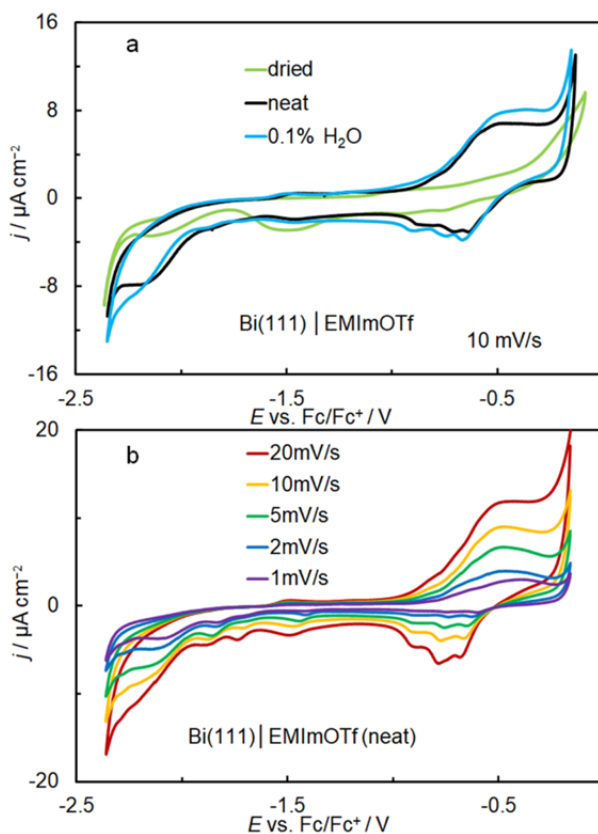


Figure 5. CVs for Bi(111) | EMImOTf interfaces: (a) dried, neat and with 0.1 % water addition (in mass fraction) and (b) neat, at different potential scan rates.

Figure 5a demonstrates the CVs for Bi(111) | EMImOTf systems measured from around -2.4 V to -0.2 V vs. Fc/Fc^+ at 10 mV/s . For the dried EMImOTf system, an electrochemically stable potential range of 2.4 V is limited by the decomposition of EMIm^+ cation at the most negative potential and by the dissolution of bismuth at the less negative potential. According to the analysis report of the manufacturer, the water concentration of neat EMImOTf is about 20 ppm . Compared with additionally dried EMImOTf, a noticeable difference in current density has been observed due to the reduction of water molecules. Somewhat higher current densities within the measured potential range can be seen when the mass fraction of water increases up to 0.1% .

Additionally, the electrochemically stable potential range becomes narrower for humid EMImOTf systems. In more detail, several faradaic peaks occur within the potential range, where the reduction of water (from -2.4 V to -1.6 V) and the adsorption processes associated with the interaction between H_2O and OTf^- (from -1.6 V to end) both contribute to the increase of the current density. The

interaction between water molecules and the $-\text{SO}_3$ group from OTf^- ions can establish the H-bonded networks condensed at the Bi(111) surface. The CVs at different scan rates (Figure 5b) give more details about the nature of these processes: (1) the reduction process related to water is irreversible; (2) the adsorption of OTf^- seems to be quasi-reversible.

The analysis of the EIS data based on the EC model in the inset of Figure 6 can provide an overview of the role of each possible process at the interface. There are two types of components in EC: resistive and capacitive components, representing high-frequency resistance (R_s), Warburg-like diffusion impedance (R_D), adsorption resistance (R_{ads}), charge transfer resistance (R_{ct}), double layer capacitance (C_{dl}), and pseudocapacitance (C_{pseudo}). Detailed descriptions of the parameters are given in the literature [125,132]. One of the main parameters, C_{dl} , describes the charge-stored ability of the system. The fitting data have a good agreement with the experimental C, E curve at 0.2 Hz (Figure 6), which indicates the sluggishness of the system. Additionally, it is necessary to note that error bars are applied to all fitting curves to show the goodness of fitting for each parameter.

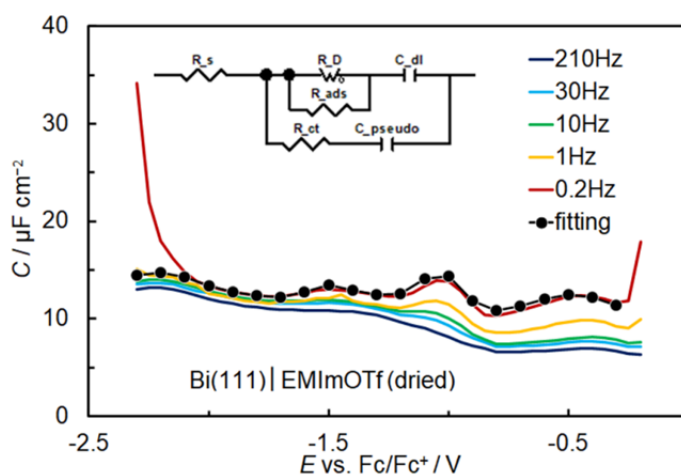


Figure 6. Capacitance (C) vs. electrode potential (E) curves at different ac frequencies and the fitting data according to EC model given in the figure.

The C_{dl}, E curves (Figure 7a) provide information on the double layer capacitance characteristics for the Bi(111) electrode in EMImOTf and its mixtures with water. Overall, the capacitance values for additionally dried EMImOTf are much lower than those for systems containing small amounts of water. The C_{dl}, E curves within the potential range from -2.3 V to -1.9 V show a consistent capacitance response, mainly explained by the adsorption of EMIm^+ ions. Compared to dried EMImOTf, the C_{dl} values for neat and 0.1% systems increase

slightly from -1.9 V to -1.0 V. The increased C_{dl} values are associated with the mixed adsorption kinetics of cations and anions. The C_{dl} values for neat and 0.1% systems increase significantly from -1.0 V to -0.1 V, which is also dependent on the water concentrations. The OTf^- ions predominantly adsorb in the first interfacial layer within this potential region. When $EMIm^+$ ions predominantly adsorb in the first interfacial layer (-2.3 V $< E < -1.6$ V), capacitance weakly depends on the water presence. The significant increase in capacitance is due to the specific adsorption of OTf^- ions interacting with water molecules, suggesting that the water molecules interact more strongly with the anion than with the cation. The water–anion bonded networks accelerate in the first ionic layer at the less negatively charged surface [144–146]. In this case, the capacitance–potential response is associated with how water strongly bonds with anion in low water concentrations.

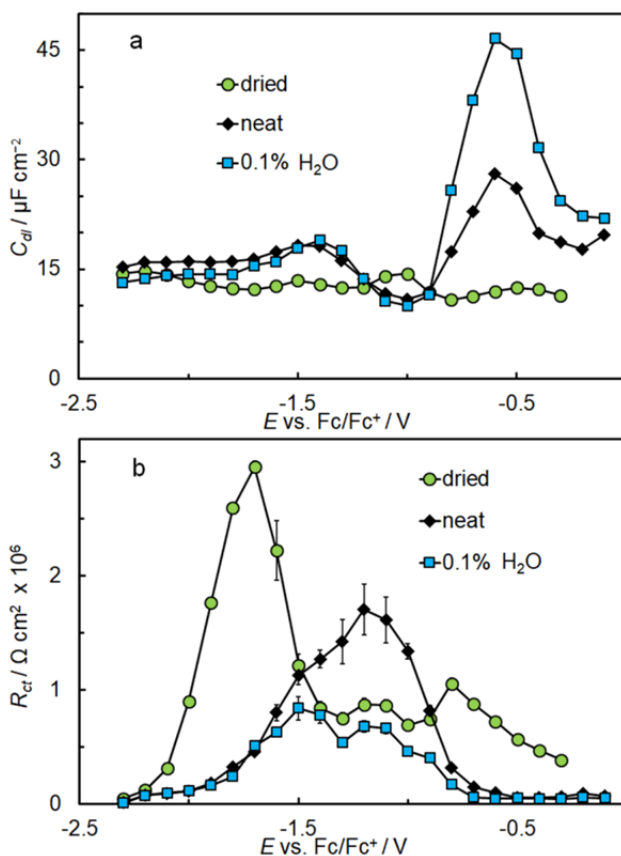


Figure 7. Double layer capacitance (C_{dl}) vs. electrode potential (E) curves (a) and charge transfer resistance (R_{ct}) vs. electrode potential (E) curves (b) for Bi(111) | EMImOTf interfaces.

The charge transfer resistance, R_{ct} , vs. potential curves (Figure 7b) provide information about the possible faradaic processes at the electrode surface. Relatively low R_{ct} values near -2.3 V imply a great possibility of the EMIm^+ reduction process. For the dried EMImOTf system, the high R_{ct} values imply that no significant faradaic process occurs within the potential range from -2 V to -1.6 V. Beyond -1.6 V, R_{ct} values decrease because OTf^- ions start to adsorb at the surface, competing with the cation desorption process.

In the case of small amounts of water, the low R_{ct} values ($E < -1.6$ V) can be explained by the irreversible water reduction process, which agrees with the CV results (seen in Figure 5). From -1.6 V to -0.9 V, R_{ct} values vary in water concentrations, which corresponds to the fewer water molecules in IL, the less possibility of the faradaic processes happening. Thus, R_{ct} values for the neat EMImOTf system are much higher than those for the 0.1% water-containing system. It suggests that a relatively stable interfacial layer structure forms in the neat system against the occurrence of faradaic processes. The interaction between water and anion directly affects the composition of interfacial layer structure because the ionic sheath (water–anion) cannot be easily broken down when the water concentration in the IL is low [144,147]. The Low R_{ct} values above -0.9 V suggest that water molecules facilitate the specific adsorption of anions, consistent with the quasi-reversible processes at the electrode surface within this potential region.

6.2. Electrochemical characteristics at Bi(*hkl*) interfaces

The discussions of the interfacial structure mainly focus on the nature of neat IL and its mixtures at the Bi(111) electrode. However, semi-metallic bismuth with three single crystal planes can perform different metallic characteristics. In addition, Because of the wide electrochemically stable potential range, the bismuth is a good choice for electrode material to study the electrochemical interface characteristics.

The CVs for Bi(*hkl*) electrodes in neat EMImOTf show a potential window of nearly 2.3 V given in Figure 8a. As described in Figure 5, the potential region of electrochemical stability is limited by the decomposition of EMIm^+ ions and the dissolution of bismuth, indicating that the dissolution of bismuth is prior to the decomposition of OTf^- ions. The reduction peaks ($E < -1.5$ V) are attributed to the reduction process of water. Thus, such small amounts of water (about 20 ppm) in EMImOTf can cause related faradaic processes [148].

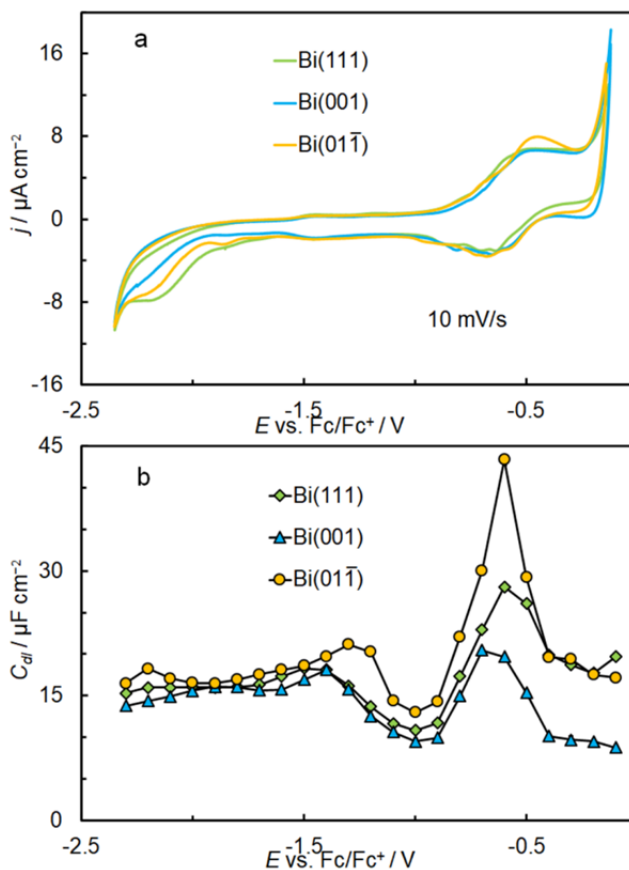


Figure 8. CVs at 10 mV/s (a) and double layer capacitance (C_{dl}) vs. potential (E) curves (b) for $\text{Bi}(hkl) \mid \text{EMImOTf}(\text{neat})$ interfaces.

Figure 8b shows the C_{dl} , E curves for $\text{Bi}(hkl) \mid \text{EMImOTf}(\text{neat})$ systems. Three C_{dl} , E curves show a similar double-humped shape. When $-2.3 \text{ V} < E < -1.4 \text{ V}$, only slightly higher C_{dl} values for the most metallic $\text{Bi}(01\bar{1})$ plane could be seen compared with $\text{Bi}(111)$ and $\text{Bi}(001)$ planes. However, when $-1.4 \text{ V} < E < -0.1 \text{ V}$, the C_{dl} values strongly depend on the electronic characteristics of each Bi single crystal plane. The capacitance peak when $-1.0 \text{ V} < E < -0.4 \text{ V}$ is due to the specific adsorption of OTf^- ions in the presence of water compared to dried EMImOTf (in Fig 6). The capacitance maxima for $\text{Bi}(hkl)$ planes increase in the order of $\text{Bi}(001) < \text{Bi}(111) < \text{Bi}(01\bar{1})$ because the differences in atomic density of each plane affect the formation of the interfacial ionic layer. The semi-metallic characteristics of $\text{Bi}(hkl)$ planes are different, i.e., the most metallic plane is $\text{Bi}(01\bar{1})$, and the other two less metallic planes are $\text{Bi}(001)$ and $\text{Bi}(111)$. The ionic layer structures at interfaces depend on the ionophilicity of the electrode materials. For example, gold has stronger ion adsorption than carbon

[149]. When $-0.4 \text{ V} < E < -0.1 \text{ V}$, the difference in capacitance response suggests that much denser interfacial layers may form on the less metallic Bi(001) plane associated with the adsorption of anions contributing to the formation of the stable layer structure.

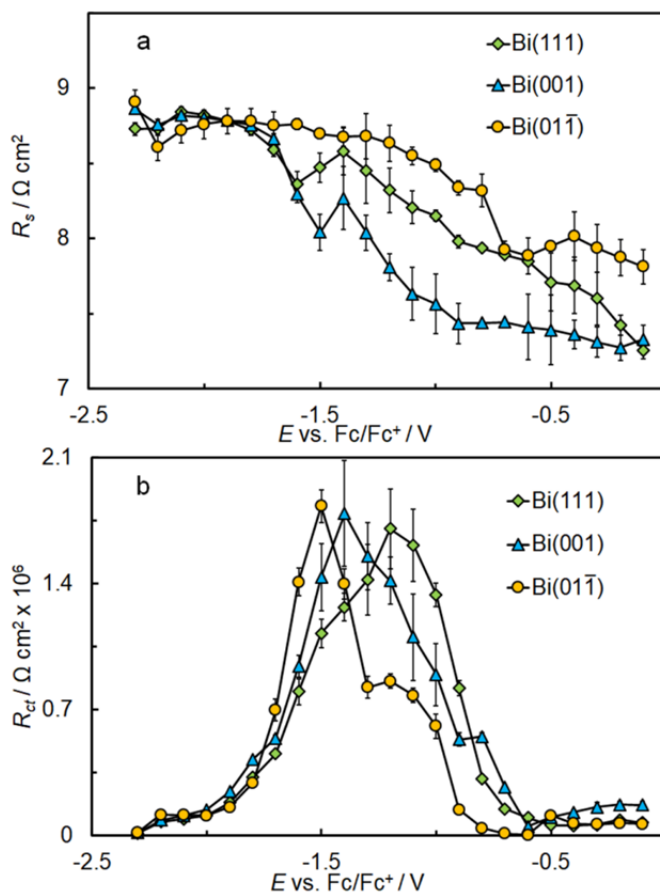


Figure 9. Series resistance (R_s) vs. potential (E) curves (a) and charge transfer resistance (R_{ct}) vs. potential (E) curves (b) for Bi(hkl) | EMImOTf (neat) interfaces.

The parameter R_s corresponds to the high-frequency series resistance and indicates the total resistance of the electrolyte solution. Figure 9a shows a potential dependence of R_s on the Bi(hkl) planes in neat EMImOTf. When $-2.3 \text{ V} < E < -1.7 \text{ V}$, the R_s , E curves for the three Bi single crystal planes are highly similar. Although the R_s values do not change much, the water reduction process occurs in this potential region. A possible explanation is a weak interaction between water and cation. Water does not affect the interfacial resistance too much when

the EMIm^+ ions preferably adsorb at the most negative potentials[144]. When $E > -1.7$ V, R_s depends on the electrode potentials applied to $\text{Bi}(hkl)$ electrodes. Thus, the strong interaction between water and anion can influence the interfacial resistance. In addition, the R_s values depend on the nature and structure of each Bi single crystal plane. The highest R_s values have been observed for the most metallic $\text{Bi}(01\bar{1})$ plane, where adsorption is strong.

The R_{ct} , E curves (Figure 9b) demonstrate the information about the possibility of faradaic processes at the surface. Generally, the shapes of the three curves are highly similar. The R_{ct} values increase first and then decrease when the electrode potentials move positively. Relatively high R_{ct} values in the vicinity of the peak potential suggest no significant charge transfer processes on the electrode surface. The peak potentials for $\text{Bi}(hkl) | \text{EMImOTf}$ (neat) interfaces can be distinguished in the following order: $\text{Bi}(01\bar{1}) < \text{Bi}(001) < \text{Bi}(111)$, suggesting that the most metallic plane $\text{Bi}(01\bar{1})$ seems to have the possibility of the charge transfer processes occurring first. Low R_{ct} values at the most negative potentials are mainly due to the water reduction process. When $E > -1.0$ V, the low R_{ct} values correspond to the specific adsorption of OTf^- ions associated with water molecules. One proof is the quasi-reversible processes (visible in the CV curves, Figure 8a) occurring in this potential range.

6.3. *In-situ* STM data at $\text{Bi}(111)$ and $\text{Bi}(01\bar{1})$ interfaces

Figure 10 shows the surface structure of the $\text{Bi}(111)$ plane in neat EMImOTf at different electrode potentials. Figure 10a shows the typical terrace structures for the $\text{Bi}(111)$ plane at -1.9 V. The terrace edges are also visible in Figures 10b and 10c, corresponding to the reactive sites of the dissolution and deposition of bismuth. Clusters on plateaus show the presence of bismuth electrodeposited from EMImOTf . A comparison of Figure 10a and Figure 10b shows that no significant surface changes occur in the potential range from -1.9 V to -1.4 V, indicating high stability of the $\text{Bi}(111) | \text{EMImOTf}$ interface, which is consistent with CV results. When the electrode potential changes to -0.9 V, clusters on plateaus gradually disappear, which is explained by the dissolution of bismuth. It is impossible to record available STM images when $E > -0.9$ V. The formation of a blocking layer limits the passage of the tunneling current, attributed to the adsorption of OTf^- ions (also indicated by the data of electrochemical measurements). Sulfonate groups of OTf^- ions interacting with Bi surface may become an obstacle for STM tip probing. When the potential moves back to -1.4 V, the initial surface structure is observed with a honeycomb-like pattern (Figure 10d). This phenomenon is due to the formation of highly ordered ionic structures that have a strong interaction with Bi atoms. The plateaus are partly covered by cationic structures and partly by anionic structures with strong adsorption at these intermediate potentials.

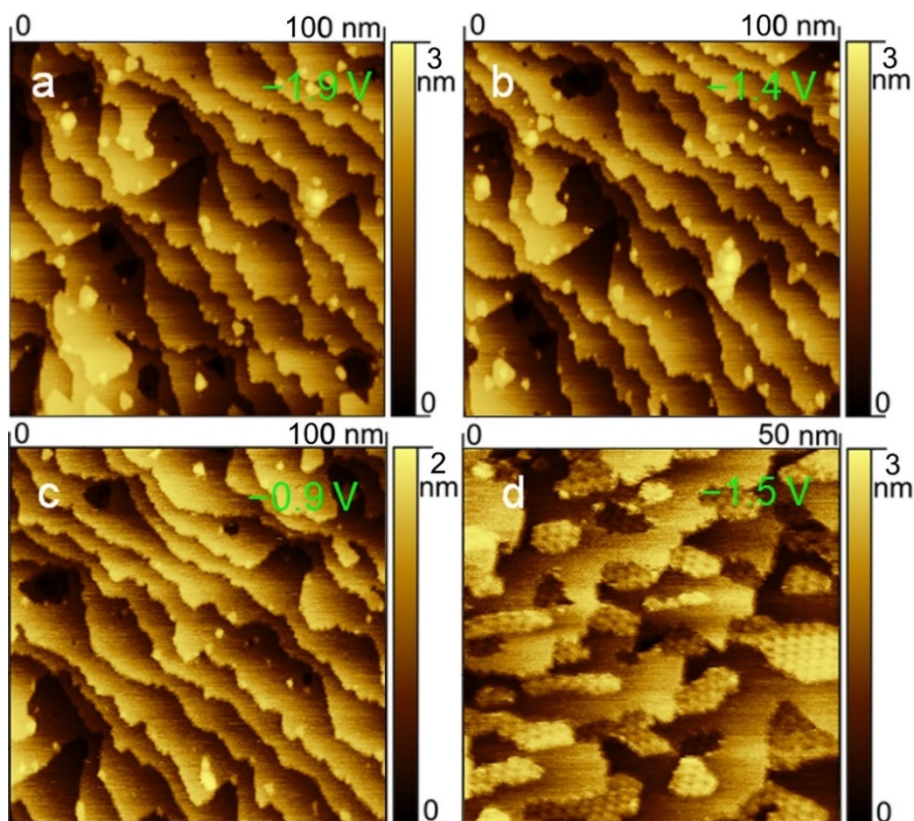


Figure 10. *In-situ* STM images for Bi(111) | EMImOTf interface at different potentials (a) -1.9 V, (b) -1.4 V, (c) -0.9 V and (d) -1.5 V (scanned back).

Figure 11 shows the *In-situ* STM images of the Bi(01 $\bar{1}$) | EMImOTf interface. Compared with other planes, the most metallic Bi(01 $\bar{1}$) surface seems more reactive and susceptible to the surface reconstruction process under polarization [150]. Figure 11a shows a striped structure of the Bi(01 $\bar{1}$) surface in EMImOTf at -2.1 V. The structures at plateaus and terrace edges seem to be more stable for the Bi(01 $\bar{1}$) interface when the surface is dominated mainly by the cations. When the electrode potential changes from -1.9 V to the less negative potentials, the terrace edges and plateaus start to reconstruct. However, a disordered structure for terrace edges and a less-striped structure for plateaus are observed in Figure 11b.

A large flat plateau is observed if the potential changes positively up to -1 V (Figure 11c). When the potential changes negatively, the plateau regions are gradually stable until a clear fine surface structure on the Bi(01 $\bar{1}$) | IL interface is seen at -1.35 V (Figure 11d). Both the pattern and the size of the fine structure depend on the electrode potential applied. The distance between signals (about 1.3 to 1.4 nm) is large enough compared to the distance between

the Bi atoms of the Bi(01 $\bar{1}$) lattice (≈ 0.4 nm). Such pattern structure correlates with the strongly adsorbed OTf⁻ ions on the Bi(01 $\bar{1}$) plane. Similar to the Bi(111) interface, it is not possible to obtain available STM images of the Bi(01 $\bar{1}$) interface When $E > -0.9$ V due to the increased noise level corresponding to the strongly adsorbed anions.

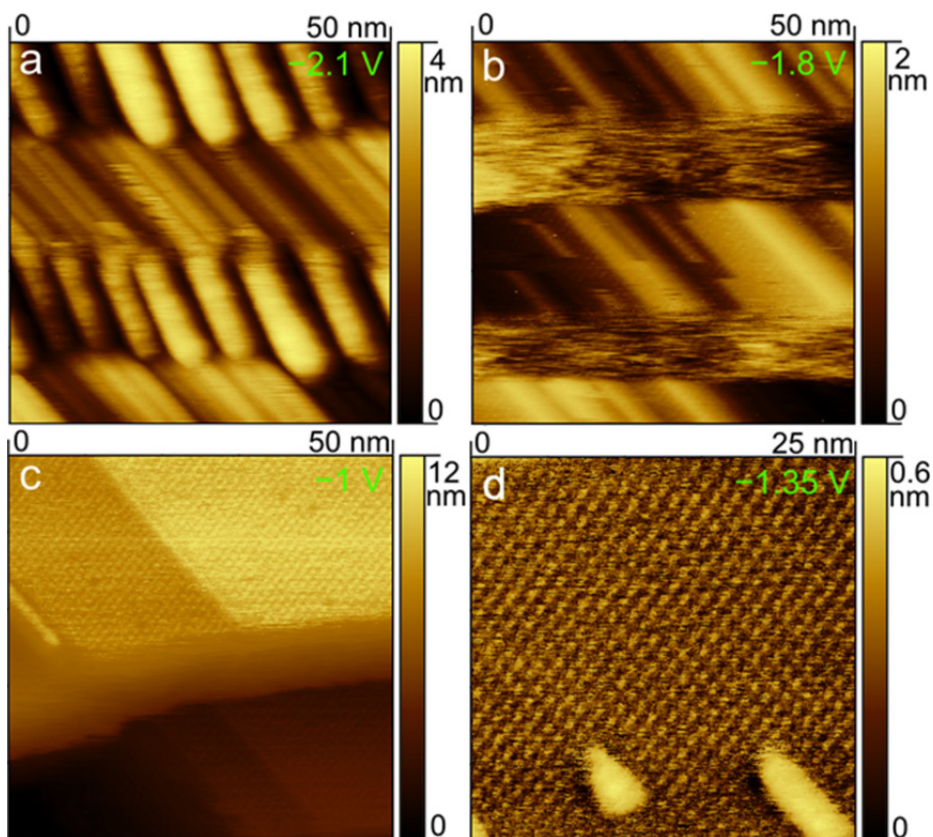


Figure 11. *In-situ* STM images of Bi(01 $\bar{1}$) | EMImOTf interface at different potentials (a) -2.1 V, (b) -1.8 V, (c) -1 V and (d) -1.35 V (scanned back).

As described above, both the honeycomb-like structure of the Bi(111) interface and the fine structure of the Bi(01 $\bar{1}$) interface are mainly due to the strong adsorption of OTf⁻ ions. In combination with electrochemistry data, the halide anions, namely bromide and iodide ions, have similar specific adsorption at the Bi(111) electrode within a less negative potential range. Therefore, STM images show the fine structure of Bi(111) surface in PMImI (Figure 12a) and EMImBF₄+20%EMImBr mixture (Figure 12b). These structures correspond to the strongly adsorbed anion layer at the Bi(111) surface.

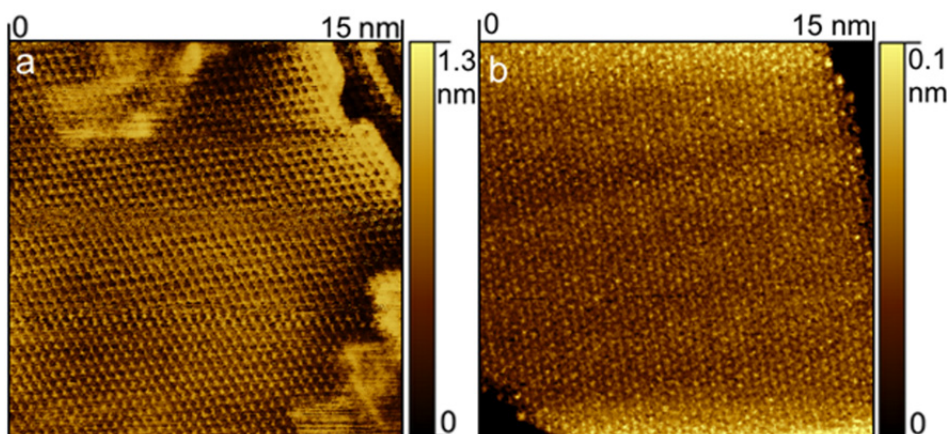


Figure 12. *In-situ* STM images at -1.1 V for interfaces: (a) $\text{Bi}(111) | \text{EMImBF}_4 + 20\% \text{EMImBr}$ and (b) $\text{Bi}(111) | \text{PMImL}$.

6.4. Energy storage characteristics of carbon electrode based supercapacitors

6.4.1. Perspective of halide ions treated supercapacitors

Both *in-situ* STM and EIS measurements have investigated the specific adsorption of halide anions. IL mixture containing halide ions applied as a promising electrolyte of SC aims to increase the capacitance. However, such electrolytes may cause several limitations for SC systems, i.e., the low operating voltage and the loss of stability and cyclability. The STM and EIS results show that the specific adsorption process of anions occurs at a limited potential range. This section applies the IL mixtures containing halide ions to impregnate the carbon electrodes instead of being directly used as electrolytes. Thus, the work of this section is on the assumption that the ions prefer to stay within or near the porous carbon electrodes by using the halide or alkali IL mixtures to treat the positive or negative carbon electrodes.

It should be mentioned that, in this section, the SC electrodes are soaked either in EMImTFSI or in EMImTFSI mixtures containing halide or alkali ions with different concentrations. The SC abbreviations corresponding to different IL mixtures are shown in Table 3.

Table 3. Abbreviations for SCs based on the corresponding electrodes treated with IL and IL salt mixtures.

SC Abbreviations	Species within negative electrode	Species within positive electrode
EMImTFSI(±)	EMIm ⁺ and TFSI ⁻	EMIm ⁺ and TFSI ⁻
EMImTFSI(-) Hal2.5(+)	EMIm ⁺ and TFSI ⁻	2.5 wt% EMIm(Cl, Br, I); EMIm ⁺ and TFSI ⁻
EMImTFSI(-) Hal5(+)	EMIm ⁺ and TFSI ⁻	5 wt% EMIm(Cl, Br, I); EMIm ⁺ and TFSI ⁻
Alk5(-) EMImTFSI(+)	5 wt% (Li, Na, K)TFSI; EMIm ⁺ and TFSI ⁻	EMIm ⁺ and TFSI ⁻
Alk5(-) Hal5(+)	5 wt% (Li, Na, K)TFSI; EMIm ⁺ and TFSI ⁻	5 wt% EMIm(Cl, Br, I); EMIm ⁺ and TFSI ⁻

6.4.2. Electrochemical analysis

6.4.2.1. Fitting of impedance data

Figure 13 shows the cell potential dependence of Nyquist plots for the Alk5(-) | Hal5(+) SC system within a wide frequency range. The EC model (in inset) consists of five elements. The additional capacitor element (C_{pseudo}) applied is only for halide ions treated systems. The series resistance, R_s , mainly describes the high-frequency resistance of the system. The diffusion resistance (R_D) derived from the Warburg element (Z_W) describes the mass-transfer limited process rate of the diffused ions. The double layer capacitance (C_{dl}) represents the total capacitance performance of SC. The charge transfer resistance (R_{ct}) represents low-frequency resistance, including slow adsorption and related faradaic processes.

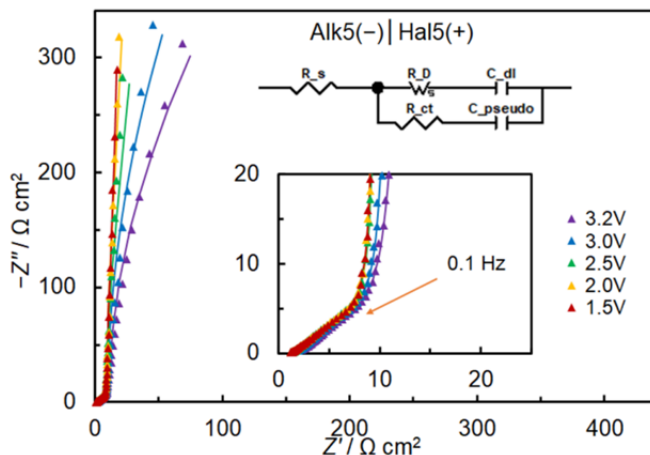


Figure 13. Nyquist plots for Alk5(-) | Hal5(+) SC system (symbols for experimental data and lines for fitting results according to an EC model given in figure).

The Nyquist plots for the Alk5(-) | Hal5(+) SC system at high and medium frequencies are not strongly dependent on the cell potentials applied. However, there is a significant dependence at low frequencies. The cell potential dependence of the Alk5(-) | Hal5(+) SC system shows the typical capacitor behaviour when $U \leq 3$ V. The Alk5(-) | Hal5(+) SC system shows good stability up to 3.2 V. When $U \geq 3.2$ V, the Nyquist plot tends to a semicircle shape at low frequencies because the cell gradually degrades due to the irreversible faradaic processes.

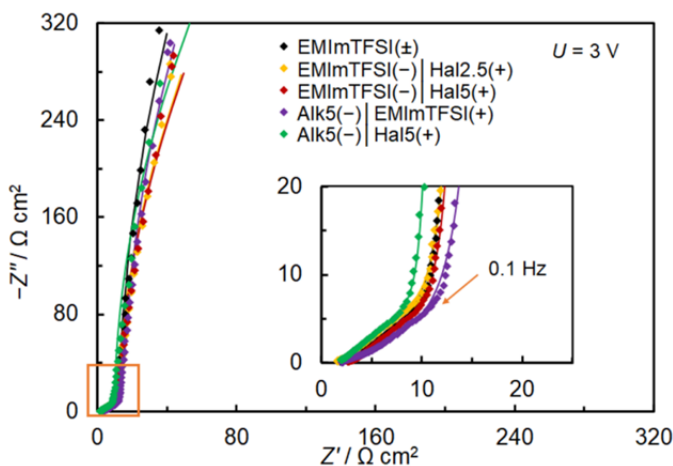


Figure 14. Nyquist plots at $U = 3$ V for SCs with electrodes treated by EMImTFSI or IL salt mixtures (symbols for experimental data and lines for fitting results).

Figure 14 shows the Nyquist plots for different systems at $U = 3\text{V}$. The nearly linear shape of Nyquist plots suggests that all SC systems behave in the typical capacitor behaviour. There is a significant difference in a high-frequency range where the $\text{Alk5(-)} \mid \text{Hal5(+)}$ SC system shows the fastest mass-transfer response while the $\text{Alk5(-)} \mid \text{EMImTFSI(+)}$ SC system demonstrates the slowest mass-transfer response.

For comparison, both capacitance and resistance values are calculated from the fitting of experimental data for different systems. Table 4 gives the resistance values for all systems at $U = 3\text{V}$ (except for R_s values at 1.5V). The R_s values are mainly dependent on the electrolyte physical properties of an interface. However, there is no significant difference in R_s values at low cell potential, which indicates a similar interface resistance behaviour for the amount and mobility of ions near the electrode from IL mixtures. In addition, the lowest R_D values for the $\text{Alk5(-)} \mid \text{Hal5(+)}$ SC system suggest the fastest mass-transfer kinetics. However, the highest R_D value for the $\text{Alk5(-)} \mid \text{EMImTFSI(+)}$ SC system suggests the slowest response to the mass-transfer process.

Table 4. Resistance parameters based on fitting of impedance data for SCs.

System	R_s ($\Omega \text{ cm}^2$)	R_D ($\Omega \text{ cm}^2$)	R_{ct} ($\Omega \text{ cm}^2$)
EMImTFSI(\pm)	1.30 \pm 0.01	13.09 \pm 0.23	3751 \pm 398
EMImTFSI(-) \mid Hal2.5(+)	1.16 \pm 0.01	23.33 \pm 0.28	3943 \pm 251
EMImTFSI(-) \mid Hal5(+)	1.11 \pm 0.01	21.62 \pm 0.23	3927 \pm 207
Alk5(-) \mid EMImTFSI(+)	2.05 \pm 0.01	31.23 \pm 0.52	6598 \pm 529
Alk5(-) \mid Hal5(+)	1.12 \pm 0.01	9.02 \pm 0.07	2339 \pm 97

Table 5. Parameters about time response and open circuit voltage for SCs.

System	OCV (mV)	Z_w T(s)	τ_R (s)
EMImTFSI(\pm)	+ 1	9.26 \pm 0.75	6.25
EMImTFSI(-) \mid Hal2.5(+)	- 38	5.23 \pm 0.22	7.34
EMImTFSI(-) \mid Hal5(+)	- 52	5.08 \pm 0.21	7.07
Alk5(-) \mid EMImTFSI(+)	+ 3	12.34 \pm 1.03	7.46
Alk5(-) \mid Hal5(+)	- 49	3.23 \pm 0.09	5.23

Table 5 shows the open circuit voltage (OCV) and time constants (Z_{W_T} and τ_R) for all SC systems. The calculation of the characteristic relaxation time constant (τ_R) is based on the imaginary capacitance vs. $\log f$ plot. τ_R describes the time response to energy storage characteristics at low and medium frequencies. The lowest τ_R value obtained from the Alk5(-) | Hal5(+) SC system suggests the quickest energy storage response. The time constant (Z_{W_T}) derived from the Warburg element demonstrates the time response to energy storage characteristics at medium frequencies. A short time response indicates that the energy storage process is related to the flexible mobilities of small-sized halide and alkali ions near/inside the carbon micro-mesopores.

6.4.2.2. Capacitive behaviour

Figure 15a presents the CVs of these SC systems at a scan rate of 5 mV/s. It should be noted that the starting potential for CVs is not applied at zero because the non-zero potential applied aims to keep the small-sized ions preferably inside the carbon pores instead of diffusing through the bulk electrolyte.

The approximately rectangular CV curves exhibit the ideally capacitive behaviour for EMImTFSI(\pm) SC system. However, these rectangular curves gradually distort for SCs with alkali or halide ions treated electrodes (Figure 15a). Small redox peaks between 0.5 V and 1.6 V are observed for the halide ions treated SC systems, suggesting the adsorption process of halide ions (Br^- and I^- ions) and the quasi-reversible redox reactions between halide ions. Correspondingly, capacitance values for halide ions treated SC systems significantly increase. This enhancement in capacitance, so-called the pseudocapacitance effect, is attributed to the specific adsorption and redox reactions of iodide ions at the carbon | iodide aqueous solution interface [133]. However, the addition of alkali ions alone (Alk5(-) | EMImTFSI(+)) does not help to increase the capacitance.

The triangular CCCD curves (Figure 15b) also show the typical capacitor behaviour for the systems studied. The CCCD curves with a linear and symmetric shape suggest a high coulombic efficiency for the halide ions treated SC systems.

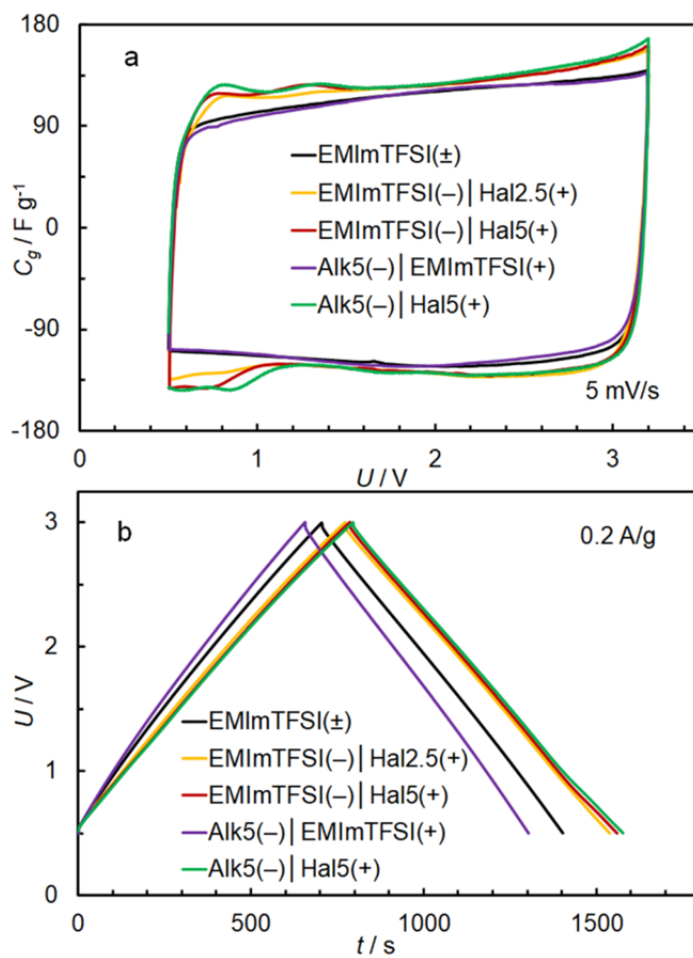


Figure 15. CVs presented as the gravimetric capacitance C_g vs. cell potential curves obtained at 5 mV/s (a) and CCCD curves recorded at 0.2 A/g (b) for different SCs.

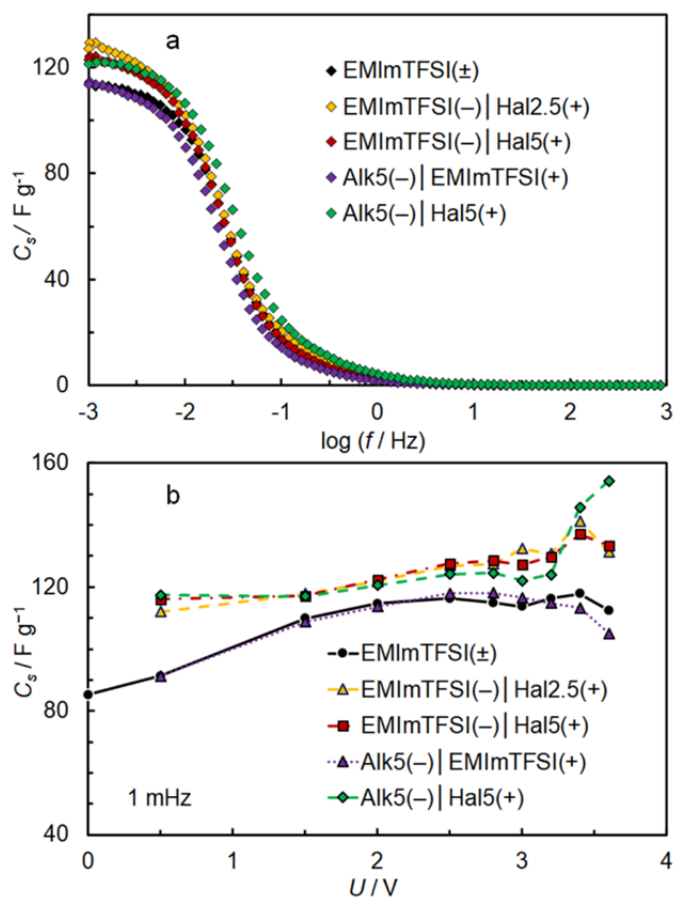


Figure 16. Series capacitance C_s vs. ac frequency plots at $U = 3 \text{ V}$ (a) and C_s vs. cell potential plots at 1 mHz (b) for SCs.

Figure 16a shows the C_s vs. $\log f$ plots for studied SC systems. A clear difference in C_s values can only be observed when $f < 1 \text{ Hz}$. The low-frequency behaviour suggests that the kinetics of the SC systems are sluggish, dominated by the slow adsorption of ions, which is consistent with rectangular CVs measured at a low scan rate. Therefore, the capacitance plateaus for all systems occur at very low frequencies. In Figure 16b, the C_s values at 1 mHz depend strongly on the SCs with different IL mixtures treated electrodes. Compared to the EMImTFSI(\pm) SC system, the halide ions treated SC systems show high C_s values. The C_s response for the EMImTFSI(\pm) and Alk5(-) | EMImTFSI(+) SC systems is similar. The high and constant C_s values for the Alk5(-) | Hal5(+) SC system are obtained within the potential range studied. The observed behaviour is likely due to the symmetric treatment methodology by the alkali ions stabilizing the negative electrode and the halide ions stabilizing the positive

electrode. In addition, an increase in capacitance ($U > 3.2$ V) corresponds to the irreversible faradaic processes of the SC system. For comparison, the Alk5(-) | EMImTFSI(+) SC system does not show any apparent improvements in capacitance.

Table 6. Comparison of SC capacitance based on data from different measurement techniques, CCD values at 0.5 A/g, CVD values at 5 mV/s, C_s values at 1 mHz, C_{dl} and C_{pseudo} values by fitting, $U = 3$ V.

System	CCD (F/g)	CVD (F/g)	C_s (F/g)	C_{dl} (F/g)	C_{pseudo} (mAh/g)
EMImTFSI(\pm)	114	115	114	115 \pm 1	/
EMImTFSI(-) Hal2.5(+)	122	121	133	125 \pm 1	51.1 \pm 13.5
EMImTFSI(-) Hal5(+)	122	121	127	121 \pm 1	52.6 \pm 13.0
Alk5(-) EMImTFSI(+)	113	110	117	115 \pm 1	/
Alk5(-) Hal5(+)	124	122	122	121 \pm 1	74.2 \pm 22.9

Table 6 shows the calculated capacitance values based on different measurement techniques. Interestingly, reproducible capacitance values are obtained from CCCD, CV, and EIS methods. By using independent measurement techniques, the EMImTFSI(\pm) SC system shows capacitance values of 114 to 115 F/g, and the Alk5(-) | Hal5(+) SC system shows capacitance values of 122 to 124 F/g. Additionally, the C_{pseudo} values presented by a unit of mAh/g show a reasonable result. The C_{pseudo} values obtained only for halide ions treated systems can interpret the capacitance enhancement by the so-called pseudocapacitive effect.

6.4.2.3. Energy behaviour

By the capacitance results, the further analysis of energy behaviour for SC systems is shown in Figures 17a and 17b. The specific energy values calculated by integrating the CCCD curves depend strongly on the cell potentials applied. Compared with the EMImTFSI(\pm) SC system, the halide ions treated SC systems show higher specific energy values. Compared with EMImTFSI(\pm) SC system, the specific energy is 10% higher for the Alk5(-) | Hal5(+) SC system, while the energy efficiency is 1.5% lower at 3.2 V. When $U \leq 3.2$ V, the overall energy efficiencies for all SC systems are approximately above 90%, likely limited by ohmic drop. However, when $U > 3.2$ V, the sharp decrease in energy efficiency is due to the irreversible faradaic processes.

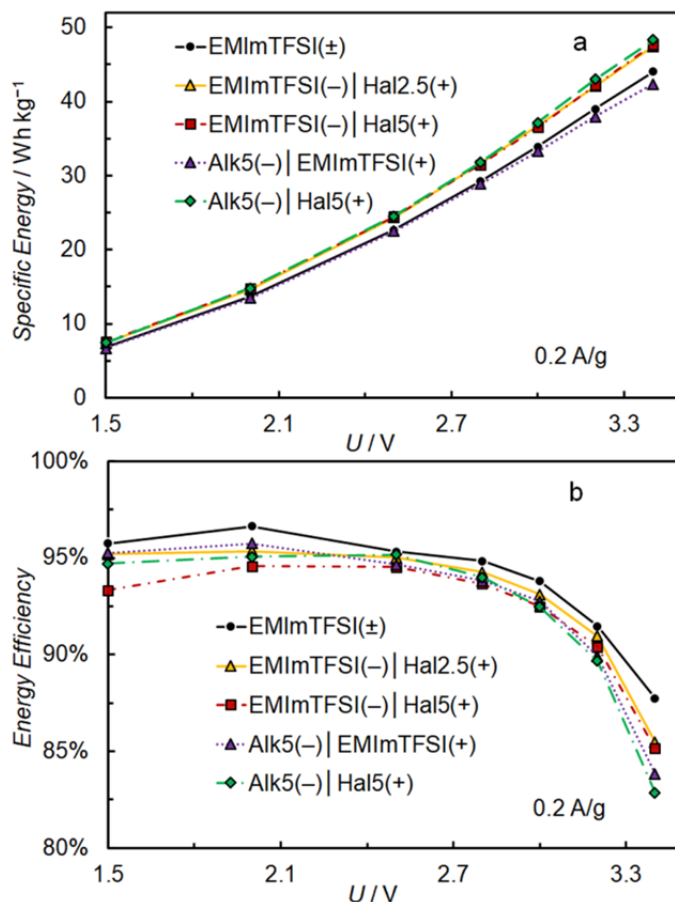


Figure 17. Specific energy vs. cell potential plots calculated from CCD data (a) and energy efficiency vs. cell potential curves based on CCCD data (b) for SCs.

6.5. Outlook: from interfacial structure to energy storage in electrochemical systems

With the development of ILs, many ILs have drawn much attention in electrolyte applications for electrochemical energy storage devices. The electrochemical application of ILs seems unable to stand firmly without understanding the interface between electrodes and ILs. Thereupon, the interfacial electrochemistry of ILs has seen extraordinary developments over the past decades due to the close connection between the electrochemical applications and the fundamentals, explored by the experimental and computer simulation techniques. The experimental findings are commonly obtained by the EIS method in combination with *in-situ* STM and other *in-situ* probe techniques [42,45,50,120,129]. With the gradual development of commercial ILs, research on ILs has

recently become more affordable and efficient. Theoretical findings in IL interface electrochemistry are also widely reported over the years [14,20,24,59,151]. However, numerous experimental and theoretical methods are applied to study interfaces, which remains a considerable challenge [152]. Thus, the new advanced experimental protocols and methodologies and data analysis procedures need to be further developed.

Currently, the EIS method is one of the most informative techniques to characterize the interface (also widely used in electroanalysis and material science) [30,153]. Many parameters related to an interface can be analysed from the impedance data, including the interfacial capacitance and resistance. For probing the interfaces, capacitance is of primary interest in the context of interfacial characteristics. Interfacial capacitance reflects some surface information, such as the formation of ionic layers, the interactions between ions and between the electrode material and ions. However, the capacitance analysis remains controversial due to the complex frequency-dependent capacitance. Thus, the EC models are widely applied to analyse and interpret the experimental impedance data. The often-used EC models built from (1) a series combination of resistor and capacitor elements and (2) a parallel combination of resistor and capacitor elements have gained wide popularity as basic combinations for analysing the electrode | electrolyte interface. It should be admitted that the use of more complex EC model and the further interpretation of the data obtained is not an easy task due to the multi-variate physical meaning of multi-element circuits.

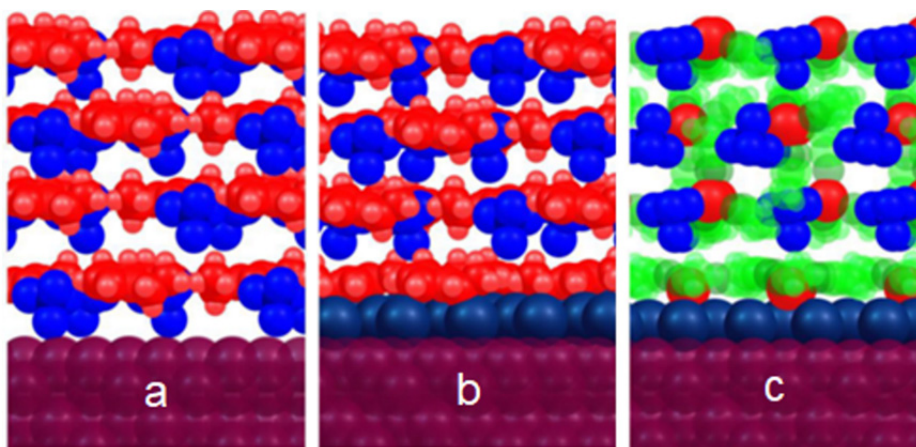


Figure 18. Graphical depiction of Bi(111) interface in (a) neat IL, (b) salt-in-IL, and (c) solvent-in-IL electrolytes at positive surface charge density (cations in red, anions in blue, neutral molecules in green, and bismuth in purple).

Based on the interface analysis, possible models of interfacial structures are constructed in ionic liquid based electrolytes at the Bi(111) electrode shown in Figure 18. Adsorption behaviour in the compact layer seems to be much stronger than in the diffuse layer in IL based electrolytes. For ILs without specifically adsorbed anions, the anions dominate in the positively charged surface. In the meantime, the role of the interaction between anions and cations is also of consideration. For IL mixtures containing specifically adsorbed anions, a dense adsorbed anion layer dominates in the positively charged surface, which agrees with the capacitance response of C , E curves.

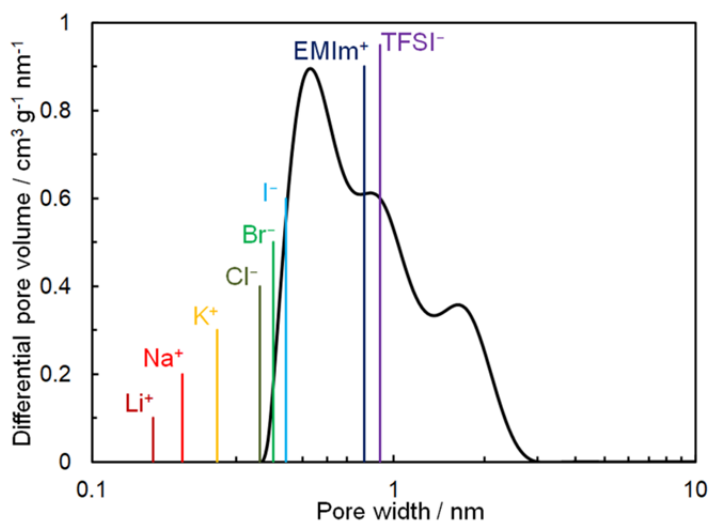


Figure 19. Differential pore size distribution vs. pore width plots for SiC-CDC material studied and the sizes of ions in the largest dimension, marked in the figure.

The properties of the electrochemical interface play a crucial role in determining the performance of electrochemical energy storage devices, such as SCs, fuel cells, batteries, and actuators. Generally, electrodes and electrolytes are the primary components for most energy storage devices. Popular materials include carbon [73,154–156], lithium [157], aluminum [158–160], zinc [161], copper [162], sodium [163–165] and potassium [166] metal electrodes. On the one hand, electrode materials used in electrochemical devices can be highly porous, different from the flat electrode used in the fundamental interface study. The size of ions from electrolyte components should be considered in correlation with the pore size of electrode materials. For example, Figure 19 shows the pore size distribution of micro- and mesoporous carbon material studied. As is seen, the adsorption process of small-sized ions can take place inside the pores and near the electrode surface. This allows us to selectively tune the porosity of an electrode material to the electrolyte and the desired electroactive components.

Current studies of the interface between electrodes and electrolytes are commonly focused on the electrode materials (i.e., Hg [31,65], Au [27,33,38,167], Pt [35,168], GC [13,26], Bi [25,64,129,132,169], Sb [46,170,171]) which are not sufficient to represent the electrode materials in practical application. For example, a high-energy-density aluminum battery is a potential alternative for post lithium battery devices. However, an electrochemically active interface between Al anode and the electrolyte still lacks fundamental explorations due to the limitation of metallic surface exposure [172,173]. Thus, the interface between electrolytes and electrode materials used in practical applications should be considered and explored further. These considerations might help to achieve the transition from fundamental interfacial behaviour and knowledge to energy storage methods applied in practical applications.

7. SUMMARY

In this thesis, the EDL structure and interfacial processes at Bi(*hkl*) planes and micro-mesoporous carbon electrodes in both ionic liquids and IL mixtures have been investigated by CV, EIS, and *in-situ* STM methods. The enhancement in capacitance at interfaces resulting from the specifically adsorbed anions in this work provides a motive to improve the capacitance performance in SC systems applied.

The CV results show the electrochemically stable potential windows for various ILs at Bi(*hkl*) planes, ions adsorption, and faradaic processes kinetics within the potential region studied. The potential regions of ideal polarizability for the Bi(111) plane for ILs were determined by the cut-off current densities limited by the decompositions of corresponding anions and cations. The narrower potential windows for ILs containing specifically adsorbed anions (PMImI, EMImMeSO₃) have been observed compared to ILs without strong specific adsorption (EMImOTf, EMImTFSI, EMImBF₄). The narrower potential windows at the Bi(111) electrode were also observed in the mixtures of EMImBF₄ + X%EMImBr. Although the wide potential window is not the whole story, the enhanced capacitances caused by the specifically adsorbed anions are key properties.

The interfacial capacitance and resistance were established by fitting the calculated impedance data to experimental ones to understand better the processes at the Bi(*hkl*) | EMImOTf interfaces. The EDL capacitance was strongly dependent on the water concentration for Bi(111) | EMImOTf interfaces when the specifically adsorbed anions dominate the positively charged surface. Besides, the EDL capacitance is also affected by the nature and surface structure of different Bi single crystal planes. The resistance parameters also show the surface kinetics of the mass-transfer and faradaic processes of the systems studied. *In-situ* STM results show a highly stable Bi(111) surface structure and an obvious reconstruction process at the Bi(01 $\bar{1}$) plane within the potential range studied. Besides, a highly ordered surface structure was observed for the Bi(01 $\bar{1}$) | EMImOTf, Bi(111) | EMImBF₄ + 20%EMImBr, and Bi(111) | PMImI systems.

To take advantage of the specific adsorption effect in the EDL capacitance, the effect of halide ions at micro-mesoporous carbon electrodes has witnessed an enhanced capacitance performance in SC systems. The SCs assembled by the carbon electrodes impregnated in halide salt mixtures (EMImTFSI + X%EMImCl/Br/I) or alkali salt mixtures (EMImTFSI + X%Li/Na/K TFSI) were studied by CV, EIS, and CCD methods. As expected, the halide ions treated SC systems showed a noticeable improvement in capacitance performance, while the alkali ions treated systems did not show such improvement. Interestingly, the symmetrically treated system (Alk5(-) | Hal5(+)) SC system showed highly constant capacitance values. Such a stable capacitance value compared to asymmetrically treated SC systems is due to the specific adsorption and redox-active properties of both I⁻ and Br⁻ ions and the symmetric doping methodology via alkali ions stabilizing the negative electrode.

8. REFERENCES

1. Fedorov, M.V.; Kornyshev, A.A. Ionic Liquids at Electrified Interfaces. *Chem. Rev.* **2014**, *114*, 2978–3036.
2. Liu, H.; Liu, Y.; Li, J. Ionic Liquids in Surface Electrochemistry. *Phys. Chem. Chem. Phys.* **2010**, *12*, 1685–1697.
3. V. Plechkova, N.; R. Seddon, K. Applications of Ionic Liquids in the Chemical Industry. *Chem. Soc. Rev.* **2008**, *37*, 123–150.
4. Watanabe, M.; Thomas, M.L.; Zhang, S.; Ueno, K.; Yasuda, T.; Dokko, K. Application of Ionic Liquids to Energy Storage and Conversion Materials and Devices. *Chem. Rev.* **2017**, *117*, 7190–7239.
5. Liu, F.; Deng, Y.; Han, X.; Hu, W.; Zhong, C. Electrodeposition of Metals and Alloys from Ionic Liquids. *J. Alloys Compd.* **2016**, *654*, 163–170.
6. Zhang, J.; Baxter, E.T.; Nguyen, M.-T.; Prabhakaran, V.; Rousseau, R.; Johnson, G.E.; Glezakou, V.-A. Structure and Stability of the Ionic Liquid Clusters [EMIM]_n[BF₄]_{N+1-} (n = 1–9): Implications for Electrochemical Separations. *J. Phys. Chem. Lett.* **2020**, *11*, 6844–6851.
7. F. Wishart, J. Energy Applications of Ionic Liquids. *Energy Environ. Sci.* **2009**, *2*, 956–961.
8. R. MacFarlane, D.; Tachikawa, N.; Forsyth, M.; M. Pringle, J.; C. Howlett, P.; D. Elliott, G.; H. Davis, J.; Watanabe, M.; Simon, P.; Austen Angell, C. Energy Applications of Ionic Liquids. *Energy Environ. Sci.* **2014**, *7*, 232–250.
9. Gale, R.J.; Osteryoung, R.A. The Electrical Double Layer at Mercury in Room Temperature Aluminum Chloride: 1-Butylpyridinium Chloride Ionic Liquids. *Electrochim. Acta* **1980**, *25*, 1527–1529.
10. Wilkes, J.S.; Levisky, J.A.; Wilson, R.A.; Hussey, C.L. Dialkylimidazolium Chloroaluminate Melts: A New Class of Room-Temperature Ionic Liquids for Electrochemistry, Spectroscopy and Synthesis. *Inorg. Chem.* **1982**, *21*, 1263–1264.
11. Zhang, S.; Sun, N.; He, X.; Lu, X.; Zhang, X. Physical Properties of Ionic Liquids: Database and Evaluation. *J. Phys. Chem. Ref. Data* **2006**, *35*, 1475–1517.
12. Li, S.; Zhang, P.; Pasquale, F.F.; Patrick, C.H.; Feng, G.; Dai, S.; Peter, T.C. Enhanced Performance of Dicationic Ionic Liquid Electrolytes by Organic Solvents. *J. Phys.: Condens. Matter* **2014**, *26*, 284105.
13. Bozym, D.J.; Uralcan, B.; Limmer, D.T.; Pope, M.A.; Szamreta, N.J.; Debenedetti, P.G.; Aksay, I.A. Anomalous Capacitance Maximum of the Glassy Carbon–Ionic Liquid Interface through Dilution with Organic Solvents. *J. Phys. Chem. Lett.* **2015**, *6*, 2644–2648.
14. Kornyshev, A.A. Double-Layer in Ionic Liquids: Paradigm Change? *J. Phys. Chem. B* **2007**, *111*, 5545–5557.
15. Islam, Md.M.; Ohsaka, T. Model of Electrical Double Layer Structure at Semi-Metallic Electrode/Ionic Liquid Interface. *Electrochim. Acta* **2021**, *368*, 137555.
16. Wang, S.; Li, S.; Cao, Z.; Yan, T. Molecular Dynamic Simulations of Ionic Liquids at Graphite Surface. *J. Phys. Chem. C* **2010**, *114*, 990–995.
17. Ruzanov, A.; Karu, K.; Ivaništšev, V.; Nazmutdinov, R.R.; Lust, E. Interplay between the Hydrophilicity of Metal Electrodes and Their Interfacial Capacitance. *Electrochim. Acta* **2016**, *210*, 615–621.
18. Addicoat, M.; Atkin, R.; Lopes, J.N.C.; Gomes, M.C.; Firestone, M.; Gardas, R.; Halstead, S.; Hardacre, C.; Hardwick, L.J.; Holbrey, J.; et al. Structure and

- Dynamics of Ionic Liquids: General Discussion. *Faraday Discuss.* **2017**, *206*, 291–337.
19. Lauw, Y.; Horne, M.D.; Rodopoulos, T.; Leermakers, F.A.M. Room-Temperature Ionic Liquids: Excluded Volume and Ion Polarizability Effects in the Electrical Double-Layer Structure and Capacitance. *Phys. Rev. Lett.* **2009**, *103*, 117801.
 20. Chen, M.; Goodwin, Z.A.H.; Feng, G.; Kornyshev, A.A. On the Temperature Dependence of the Double Layer Capacitance of Ionic Liquids. *J. Electroanal. Chem.* **2018**, *819*, 347–358.
 21. Lynden-Bell, R.M.; Frolov, A.I.; Fedorov, M.V. Electrode Screening by Ionic Liquids. *Phys. Chem. Chem. Phys.* **2012**, *14*, 2693–2701.
 22. Uysal, A.; Zhou, H.; Feng, G.; Lee, S.S.; Li, S.; Fenter, P.; Cummings, P.T.; Fulvio, P.F.; Dai, S.; McDonough, J.K.; et al. Structural Origins of Potential Dependent Hysteresis at the Electrified Graphene/Ionic Liquid Interface. *J. Phys. Chem. C* **2014**, *118*, 569–574.
 23. Paek, E.; Pak, A.J.; Hwang, G.S. A Computational Study of the Interfacial Structure and Capacitance of Graphene in [BMIM][PF6] Ionic Liquid. *J. Electrochem. Soc.* **2012**, *160*, A1–A10.
 24. Hu, Z.; Vatamanu, J.; Borodin, O.; Bedrov, D. A Molecular Dynamics Simulation Study of the Electric Double Layer and Capacitance of [BMIM][PF6] and [BMIM][BF4] Room Temperature Ionic Liquids near Charged Surfaces. *Phys. Chem. Chem. Phys.* **2013**, *15*, 14234–14247.
 25. Siinor, L.; Lust, K.; Lust, E. Influence of Anion Composition and Size on the Double Layer Capacitance for Bi(111)|room Temperature Ionic Liquid Interface. *Electrochem. commun.* **2010**, *12*, 1058–1061.
 26. Lockett, V.; Sedev, R.; Ralston, J.; Horne, M.; Rodopoulos, T. Differential Capacitance of the Electrical Double Layer in Imidazolium-Based Ionic Liquids: Influence of Potential, Cation Size, and Temperature. *J. Phys. Chem. C* **2008**, *112*, 7486–7495.
 27. Alam, M.T.; Masud, J.; Islam, Md.M.; Okajima, T.; Ohsaka, T. Differential Capacitance at Au(111) in 1-Alkyl-3-Methylimidazolium Tetrafluoroborate Based Room-Temperature Ionic Liquids. *J. Phys. Chem. C* **2011**, *115*, 19797–19804.
 28. Silva, F.; Gomes, C.; Figueiredo, M.; Costa, R.; Martins, A.; Pereira, C.M. The Electrical Double Layer at the [BMIM][PF6] Ionic Liquid/Electrode Interface – Effect of Temperature on the Differential Capacitance. *J. Electroanal. Chem.* **2008**, *622*, 153–160.
 29. Jitvisate, M.; Seddon, J.R.T. Direct Measurement of the Differential Capacitance of Solvent-Free and Dilute Ionic Liquids. *J. Phys. Chem. Lett.* **2018**, *9*, 126–131.
 30. Pajkossy, T.; Jurczakowski, R. Electrochemical Impedance Spectroscopy in Interfacial Studies. *Curr. Opin. Electrochem.* **2017**, *1*, 53–58.
 31. Alam, M.T.; Mominul Islam, Md.; Okajima, T.; Ohsaka, T. Measurements of Differential Capacitance in Room Temperature Ionic Liquid at Mercury, Glassy Carbon and Gold Electrode Interfaces. *Electrochem. commun.* **2007**, *9*, 2370–2374.
 32. Roling, B.; Drüsichler, M.; Huber, B. Slow and Fast Capacitive Process Taking Place at the Ionic Liquid/Electrode Interface. *Faraday Discuss.* **2011**, *154*, 303–311.
 33. Vargas-Barbosa, N.M.; Roling, B. Time-Resolved Determination of the Potential of Zero Charge at Polycrystalline Au/Ionic Liquid Interfaces. *J. Chem. Phys.* **2018**, *148*, 193820.

34. Costa, R.; Pereira, C.M.; Fernando Silva, A. Structural Ordering Transitions in Ionic Liquids Mixtures. *Electrochem. commun.* **2015**, *57*, 10–13.
35. Costa, R.; Pereira, C.M.; Silva, A.F. Charge Storage on Ionic Liquid Electric Double Layer: The Role of the Electrode Material. *Electrochim. Acta* **2015**, *167*, 421–428.
36. Zhou, W.; Inoue, S.; Iwahashi, T.; Kanai, K.; Seki, K.; Miyamae, T.; Kim, D.; Katayama, Y.; Ouchi, Y. Double Layer Structure and Adsorption/Desorption Hysteresis of Neat Ionic Liquid on Pt Electrode Surface — an in-Situ IR-Visible Sum-Frequency Generation Spectroscopic Study. *Electrochem. commun.* **2010**, *12*, 672–675.
37. Iwahashi, T.; Ishiyama, T.; Sakai, Y.; Morita, A.; Kim, D.; Ouchi, Y. Bi-Layering at Ionic Liquid Surfaces: A Sum-Frequency Generation Vibrational Spectroscopy- and Molecular Dynamics Simulation-Based Study. *Phys. Chem. Chem. Phys.* **2020**, *22*, 12565–12576.
38. Hayes, R.; Borisenko, N.; Tam, M.K.; Howlett, P.C.; Endres, F.; Atkin, R. Double Layer Structure of Ionic Liquids at the Au(111) Electrode Interface: An Atomic Force Microscopy Investigation. *J. Phys. Chem. C* **2011**, *115*, 6855–6863.
39. Tsai, W.-Y.; Come, J.; Zhao, W.; Wang, R.; Feng, G.; Prasad Thapaliya, B.; Dai, S.; Collins, L.; Balke, N. Hysteretic Order-Disorder Transitions of Ionic Liquid Double Layer Structure on Graphite. *Nano Energy* **2019**, *60*, 886–893.
40. Umeda, K.; Kobayashi, K.; Minato, T.; Yamada, H. Molecular-Scale Solvation Structures of Ionic Liquids on a Heterogeneously Charged Surface. *J. Phys. Chem. Lett.* **2020**, *11*, 8094–8099.
41. Borisenko, N.; Lahiri, A.; Pulletikurthi, G.; Cui, T.; Carstens, T.; Zahlbach, J.; Atkin, R.; Endres, F. The Au(111)/IL Interfacial Nanostructure in the Presence of Precursors and Its Influence on the Electrodeposition Process. *Faraday Discuss.* **2018**, *206*, 459–473.
42. Atkin, R.; Borisenko, N.; Drüscher, M.; Abedin, S.Z.E.; Endres, F.; Hayes, R.; Huber, B.; Roling, B. An in Situ STM/AFM and Impedance Spectroscopy Study of the Extremely Pure 1-Butyl-1-Methylpyrrolidinium Tris(Pentafluoroethyl)Trifluorophosphate/Au(111) Interface: Potential Dependent Solvation Layers and the Herringbone Reconstruction. *Phys. Chem. Chem. Phys.* **2011**, *13*, 6849–6857.
43. Liu, S.; Peng, J.; Chen, L.; Sebastián, P.; Feliu, J.M.; Yan, J.; Mao, B. In-Situ STM and AFM Studies on Electrochemical Interfaces in Imidazolium-Based Ionic Liquids. *Electrochim. Acta* **2019**, *309*, 11–17.
44. Rudnev, A.V.; Ehrenburg, M.R.; Molodkina, E.B.; Abdelrahman, A.; Arenz, M.; Broekmann, P.; Jacob, T. Structural Changes of Au(111) Single Crystal Electrode Surface in Ionic Liquids. *ChemElectroChem* **2020**, *7*, 501–508.
45. Anderson, E.; Grozovski, V.; Siinor, L.; Siimenson, C.; Ivaništšev, V.; Lust, K.; Kallip, S.; Lust, E. Influence of the Electrode Potential and in Situ STM Scanning Conditions on the Phase Boundary Structure of the Single Crystal Bi(111)|1-Butyl-4-Methylpyridinium Tetrafluoroborate Interface. *J. Electroanal. Chem.* **2013**, *709*, 46–56.
46. Pikma, P.; Siinor, L.; Oll, O.; Lust, E. Formation of 2,2'-Bipyridine Adlayers at Sb(111)|ionic Liquid+2,2'-Bipyridine Solution Interface. *Electrochem. commun.* **2015**, *61*, 61–65.
47. Endres, F.; Borisenko, N.; Abedin, S.Z.E.; Hayes, R.; Atkin, R. The Interface Ionic Liquid(s)/Electrode(s): In Situ STM and AFM Measurements. *Faraday Discuss.* **2011**, *154*, 221–233.

48. Su, Y.-Z.; Fu, Y.-C.; Yan, J.-W.; Chen, Z.-B.; Mao, B.-W. Double Layer of Au(100)/Ionic Liquid Interface and Its Stability in Imidazolium-Based Ionic Liquids. *Angew. Chem. Int. Ed.* **2009**, *48*, 5148–5151.
49. Yan, J.-W.; Tian, Z.-Q.; Mao, B.-W. Molecular-Level Understanding of Electric Double Layer in Ionic Liquids. *Curr. Opin. Electrochem.* **2017**, *4*, 105–111.
50. Pajkossy, T.; Müller, C.; Jacob, T. The Metal–Ionic Liquid Interface as Characterized by Impedance Spectroscopy and in Situ Scanning Tunneling Microscopy. *Phys. Chem. Chem. Phys.* **2018**, *20*, 21241–21250.
51. Drüscler, M.; Borisenko, N.; Wallauer, J.; Winter, C.; Huber, B.; Endres, F.; Roling, B. New Insights into the Interface between a Single-Crystalline Metal Electrode and an Extremely Pure Ionic Liquid : Slow Interfacial Processes and the Influence of Temperature on Interfacial Dynamics. *Phys. Chem. Chem. Phys.* **2012**, *14*, 5090–5099.
52. Helmholtz, H. Ueber Einige Gesetze Der Vertheilung Elektrischer Ströme in Körperlichen Leitern Mit Anwendung Auf Die Thierisch-Elektrischen Versuche. *Ann. Phys.* **1853**, *165*, 211–233.
53. Gouy, M. Sur La Constitution de La Charge Électrique à La Surface d'un Électrolyte. *Journal de Physique Théorique et Appliquée* **1910**, *9*, 457–468.
54. Chapman, D.L. LI. A Contribution to the Theory of Electrocapillarity. *Philosophical Magazine Series 6* **1913**, *25*, 475–481.
55. Stern, O. Zur Theorie Der Elektrolytischen Doppelschicht. *Zeitschrift für Elektrochemie und angewandte physikalische Chemie* **1924**, *30*, 508–516.
56. Grahame, D.C. The Electrical Double Layer and the Theory of Electrocapillarity. *Chem. Rev.* **1947**, *41*, 441–501.
57. Bockris, J.O.; Devanathan, M. a. V.; Müller, K.; Butler, J.A.V. On the Structure of Charged Interfaces. *Proc. R. Soc.* **1963**, *274*, 55–79.
58. Oldham, K.B. A Gouy–Chapman–Stern Model of the Double Layer at a (Metal)/(Ionic Liquid) Interface. *J. Electroanal. Chem.* **2008**, *613*, 131–138.
59. Bazant, M.Z.; Storey, B.D.; Kornyshev, A.A. Double Layer in Ionic Liquids: Overscreening versus Crowding. *Phys. Rev. Lett.* **2011**, *106*, 046102.
60. Kornyshev, A.A.; Luque, N.B.; Schmickler, W. Differential Capacitance of Ionic Liquid Interface with Graphite: The Story of Two Double Layers. *J. Solid State Electrochem.* **2014**, *18*, 1345–1349.
61. Lauw, Y.; Horne, M.D.; Rodopoulos, T.; Nelson, A.; Leermakers, F.A.M. Electrical Double-Layer Capacitance in Room Temperature Ionic Liquids: Ion-Size and Specific Adsorption Effects. *J. Phys. Chem. B* **2010**, *114*, 11149–11154.
62. Lockett, V.; Horne, M.; Sedev, R.; Rodopoulos, T.; Ralston, J. Differential Capacitance of the Double Layer at the Electrode/Ionic Liquids Interface. *Phys. Chem. Chem. Phys.* **2010**, *12*, 12499–12512.
63. Siinor, L.; Lust, K.; Lust, E. Electrical Double Layer Capacitance at Bi (111) | 1 - Ethyl-3-Methylimidazolium Tetrafluoroborate Interface as a Function of the Electrode Potential. *J. Electrochem. Soc.* **2010**, *157*, F83–F87.
64. Siinor, L.; Arendi, R.; Lust, K.; Lust, E. Influence of Temperature on the Electrochemical Characteristics of Bi(111)|ionic Liquid Interface. *J. Electroanal. Chem.* **2013**, *689*, 51–56.
65. Nanjundiah, C.; McDevitt, S.F.; Koch, V.R. Differential Capacitance Measurements in Solvent-Free Ionic Liquids at Hg and C Interfaces. *J. Electrochem. Soc.* **1997**, *144*, 3392.

66. Siinor, L.; Siimenson, C.; Ivaništšev, V.; Lust, K.; Lust, E. Influence of Cation Chemical Composition and Structure on the Double Layer Capacitance for Bi(111)|room Temperature Ionic Liquid Interface. *J. Electroanal. Chem.* **2012**, *668*, 30–36.
67. Lust, K.; Lust, E. Influence of Geometrical Structure of the Anions on the Adsorption Parameters at the Bi(001) Electrode. *J. Electroanal. Chem.* **2003**, *552*, 129–139.
68. Oll, O.; Romann, T.; Siimenson, C.; Lust, E. Influence of Chemical Composition of Electrode Material on the Differential Capacitance Characteristics of the Ionic Liquid|electrode Interface. *Electrochem. commun.* **2017**, *82*, 39–42.
69. Siinor, L.; Poom, J.; Siimenson, C.; Lust, K.; Lust, E. Electrochemical Characteristics Pyrolytic Graphite|mixture of 1-Ethyl-3-Methylimidazolium Tetrafluoroborate and 1-Ethyl-3-Methylimidazolium Iodide Interface. *J. Electroanal. Chem.* **2014**, *719*, 133–137.
70. Oll, O.; Siimenson, C.; Lust, K.; Gorbatovski, G.; Lust, E. Specific Adsorption from an Ionic Liquid: Impedance Study of Iodide Ion Adsorption from a Pure Halide Ionic Liquid at Bismuth Single Crystal Planes. *Electrochimica Acta* **2017**, *247*, 910–919.
71. Balducci, A. Electrolytes for High Voltage Electrochemical Double Layer Capacitors: A Perspective Article. *J. Power Sources* **2016**, *326*, 534–540.
72. Salanne, M.; Rotenberg, B.; Naoi, K.; Kaneko, K.; Taberna, P.-L.; Grey, C.P.; Dunn, B.; Simon, P. Efficient Storage Mechanisms for Building Better Supercapacitors. *Nat. Energy* **2016**, *1*, 16070.
73. Béguin, F.; Presser, V.; Balducci, A.; Frackowiak, E. Carbons and Electrolytes for Advanced Supercapacitors. *Adv. Mater.* **2014**, *26*, 2219–2251.
74. Largeot, C.; Portet, C.; Chmiola, J.; Taberna, P.-L.; Gogotsi, Y.; Simon, P. Relation between the Ion Size and Pore Size for an Electric Double-Layer Capacitor. *J. Am. Chem. Soc.* **2008**, *130*, 2730–2731.
75. Lin, R.; Huang, P.; Ségalini, J.; Largeot, C.; Taberna, P.L.; Chmiola, J.; Gogotsi, Y.; Simon, P. Solvent Effect on the Ion Adsorption from Ionic Liquid Electrolyte into Sub-Nanometer Carbon Pores. *Electrochim. Acta* **2009**, *54*, 7025–7032.
76. Härmas, R.; Palm, R.; Härmas, M.; Pohl, M.; Kurig, H.; Tallo, I.; Tee, E.; Vaas, I.; Väli, R.; Romann, T.; et al. Influence of Porosity Parameters and Electrolyte Chemical Composition on the Power Densities of Non-Aqueous and Ionic Liquid Based Supercapacitors. *Electrochim. Acta* **2018**, *283*, 931–948.
77. Li, W.; Liu, J.; Zhao, D. Mesoporous Materials for Energy Conversion and Storage Devices. *Nat. Rev. Mater.* **2016**, *1*, 1–17.
78. Frackowiak, E.; Abbas, Q.; Béguin, F. Carbon/Carbon Supercapacitors. *J. Energy Chem.* **2013**, *22*, 226–240.
79. Lin, R.; Taberna, P.-L.; Fantini, S.; Presser, V.; Pérez, C.R.; Malbosc, F.; Rupesinghe, N.L.; Teo, K.B.K.; Gogotsi, Y.; Simon, P. Capacitive Energy Storage from –50 to 100 °C Using an Ionic Liquid Electrolyte. *J. Phys. Chem. Lett.* **2011**, *2*, 2396–2401.
80. Kurig, H.; Vestli, M.; Jänes, A.; Lust, E. Electrical Double Layer Capacitors Based on Two 1-Ethyl-3-Methylimidazolium Ionic Liquids with Different Anions. *Electrochem. Solid-State Lett.* **2011**, *14*, A120–A122.
81. Forse, A.C.; Griffin, J.M.; Merlet, C.; Bayley, P.M.; Wang, H.; Simon, P.; Grey, C.P. NMR Study of Ion Dynamics and Charge Storage in Ionic Liquid Supercapacitors. *J. Am. Chem. Soc.* **2015**, *137*, 7231–7242.

82. Tee, E.; Tallo, I.; Thomberg, T.; Jänes, A.; Lust, E. Supercapacitors Based on Activated Silicon Carbide-Derived Carbon Materials and Ionic Liquid. *J. Electrochem. Soc.* **2016**, *163*, A1317–A1325.
83. Sillars, F.B.; Fletcher, S.I.; Mirzaeian, M.; Hall, P.J. Variation of Electrochemical Capacitor Performance with Room Temperature Ionic Liquid Electrolyte Viscosity and Ion Size. *Phys. Chem. Chem. Phys.* **2012**, *14*, 6094–6100.
84. Brandt, A.; Pohlmann, S.; Varzi, A.; Balducci, A.; Passerini, S. Ionic Liquids in Supercapacitors. *MRS Bull.* **2013**, *38*, 554–559.
85. Lian, C.; Liu, K.; Van Aken, K.L.; Gogotsi, Y.; Wesolowski, D.J.; Liu, H.L.; Jiang, D.E.; Wu, J.Z. Enhancing the Capacitive Performance of Electric Double-Layer Capacitors with Ionic Liquid Mixtures. *ACS Energy Lett.* **2016**, *1*, 21–26.
86. Akinwolemiwa, B.; Peng, C.; Chen, G.Z. Redox Electrolytes in Supercapacitors. *J. Electrochem. Soc.* **2015**, *162*, A5054–A5059.
87. Xie, H.J.; Gélinas, B.; Rochefort, D. Redox-Active Electrolyte Supercapacitors Using Electroactive Ionic Liquids. *Electrochem. commun.* **2016**, *66*, 42–45.
88. You, D.-J.; Yin, Z.; Ahn, Y.; Lee, S.-H.; Yoo, J.; Kim, Y.S. Redox-Active Ionic Liquid Electrolyte with Multi Energy Storage Mechanism for High Energy Density Supercapacitor. *RSC Adv.* **2017**, *7*, 55702–55708.
89. Frackowiak, E.; Meller, M.; Menzel, J.; Gastol, D.; Fic, K. Redox-Active Electrolyte for Supercapacitor Application. *Faraday Discuss.* **2014**, *172*, 179–198.
90. Yu, L.; Chen, G.Z. Redox Electrode Materials for Supercapatteries. *J. Power Sources* **2016**, *326*, 604–612.
91. Béguin, F.; Szostak, K.; Lota, G.; Frackowiak, E. A Self-Supporting Electrode for Supercapacitors Prepared by One-Step Pyrolysis of Carbon Nanotube/Polyacrylonitrile Blends. *Adv. Mater.* **2005**, *17*, 2380–2384.
92. Fleischmann, S.; Mitchell, J.B.; Wang, R.; Zhan, C.; Jiang, D.; Presser, V.; Augustyn, V. Pseudocapacitance: From Fundamental Understanding to High Power Energy Storage Materials. *Chem. Rev.* **2020**, *120*, 6738–6782.
93. Lozano-Castelló, D.; Cazorla-Amorós, D.; Linares-Solano, A.; Shiraishi, S.; Kurihara, H.; Oya, A. Influence of Pore Structure and Surface Chemistry on Electric Double Layer Capacitance in Non-Aqueous Electrolyte. *Carbon* **2003**, *41*, 1765–1775.
94. Momma, T.; Liu, X.; Osaka, T.; Ushio, Y.; Sawada, Y. Electrochemical Modification of Active Carbon Fiber Electrode and Its Application to Double-Layer Capacitor. *J. Power Sources* **1996**, *60*, 249–253.
95. Chmiola, J.; Yushin, G.; Gogotsi, Y.; Portet, C.; Simon, P.; Taberna, P.L. Anomalous Increase in Carbon Capacitance at Pore Sizes Less Than 1 Nanometer. *Science* **2006**, *313*, 1760–1763.
96. Segalini, J.; Iwama, E.; Taberna, P.-L.; Gogotsi, Y.; Simon, P. Steric Effects in Adsorption of Ions from Mixed Electrolytes into Microporous Carbon. *Electrochem. commun.* **2012**, *15*, 63–65.
97. Lota, G.; Fic, K.; Frackowiak, E. Alkali Metal Iodide/Carbon Interface as a Source of Pseudocapacitance. *Electrochem. commun.* **2011**, *13*, 38–41.
98. Tooming, T.; Thomberg, T.; Siinor, L.; Tõnurist, K.; Jänes, A.; Lust, E. A Type High Capacitance Supercapacitor Based on Mixed Room Temperature Ionic Liquids Containing Specifically Adsorbed Iodide Anions. *J. Electrochem. Soc.* **2014**, *161*, A222–A227.
99. Yamazaki, S.; Ito, T.; Yamagata, M.; Ishikawa, M. Non-Aqueous Electrochemical Capacitor Utilizing Electrolytic Redox Reactions of Bromide Species in Ionic Liquid. *Electrochim. Acta* **2012**, *86*, 294–297.

100. Thomberg, T.; Lust, E.; Jänes, A. Iodide Ion Containing Ionic Liquid Mixture Based Asymmetrical Capacitor Performance. *J. Energy Storage* **2020**, *32*, 101845.
101. Weaver, J.E.F.; Breadner, D.; Deng, F.; Ramjee, B.; Ragogna, P.J.; Murray, R.W. Electrochemistry of Ferrocene-Functionalized Phosphonium Ionic Liquids. *J. Phys. Chem. C* **2011**, *115*, 19379–19385.
102. Sun, G.; Li, K.; Sun, C. Electrochemical Performance of Electrochemical Capacitors Using Cu(II)-Containing Ionic Liquid as the Electrolyte. *Microporous Mesoporous Mater.* **2010**, *128*, 56–61.
103. Zhang, S.; Bo, Z.; Yang, H.; Yang, J.; Duan, L.; Yan, J.; Cen, K. Insights into the Effects of Solvent Properties in Graphene Based Electric Double-Layer Capacitors with Organic Electrolytes. *J. Power Sources* **2016**, *334*, 162–169.
104. Frackowiak, E.; Fic, K.; Meller, M.; Lota, G. Electrochemistry Serving People and Nature: High-Energy Ecocapacitors Based on Redox-Active Electrolytes. *Chem SusChem* **2012**, *5*, 1181–1185.
105. Mann, L.; Voßnacker, P.; Müller, C.; Riedel, S. [NMe₄][I4Br₅]: A New Iodobromide from an Ionic Liquid with Halogen–Halogen Interactions. *Chem. Eur. J.* **2017**, *23*, 244–249.
106. Haller, H.; Riedel, S. Recent Discoveries of Polyhalogen Anions – from Bromine to Fluorine. *Z. Anorg. Allg. Chem.* **2014**, *640*, 1281–1291.
107. Bard, A.J.; Faulkner, L.R. *Electrochemical Methods: Fundamentals and Applications*. Wiley **2000**.
108. Wang, J. *Analytical Electrochemistry*. Wiley **2006**.
109. Laheäär, A.; Przygocki, P.; Abbas, Q.; Béguin, F. Appropriate Methods for Evaluating the Efficiency and Capacitive Behavior of Different Types of Supercapacitors. *Electrochem. commun.* **2015**, *60*, 21–25.
110. Lasia, A. Electrochemical Impedance Spectroscopy and Its Applications. In *Springer: Boston* **2002**, pp. 143–248.
111. Bard, A.J.; Stratmann, M. *Encyclopedia of Electrochemistry*. Wiley **2007**.
112. Binnig, G.; Rohrer, H.; Gerber, Ch.; Weibel, E. Surface Studies by Scanning Tunneling Microscopy. *Phys. Rev. Lett.* **1982**, *49*, 57–61.
113. Mironov, V.L. *Fundamentals of Scanning Probe Microscopy. NT-MDT: Nizhniy Novgorod* **2004**.
114. Frommer, J. Scanning Tunneling Microscopy and Atomic Force Microscopy in Organic Chemistry. *Angew. Chem. Int. Ed.* **1992**, *31*, 1298–1328.
115. Yagati, A.K.; Min, J.; Choi, J.-W. Electrochemical Scanning Tunneling Microscopy (ECSTM) – From Theory to Future Applications. *IntechOpen* **2014**.
116. Wiesendanger, R.; Güntherodt, H.-J. *Scanning Tunneling Microscopy II: Further Applications and Related Scanning Techniques. Springer-Verlag: Berlin Heidelberg* **1992**.
117. Itaya, K. In Situ Scanning Tunneling Microscopy in Electrolyte Solutions. *Prog. Surf. Sci.* **1998**, *58*, 121–247.
118. Feng, H.; Xu, X.; Du, Y.; Dou, S.X. Application of Scanning Tunneling Microscopy in Electrocatalysis and Electrochemistry. *Electrochem. Energ. Rev.* **2021**, *4*, 249–268.
119. Grozovski, V.; Ivaništšev, V.; Kasuk, H.; Romann, T.; Lust, E. Balance of the Interfacial Interactions of 4,4'-Bipyridine at Bi(111) Surface. *Electrochim. Acta* **2014**, *120*, 86–95.

120. Anderson, E.; Grozovski, V.; Siinor, L.; Siimenson, C.; Lust, E. In Situ STM Studies of Bi(111)|1-Ethyl-3-Methylimidazolium Tetrafluoroborate+1-Ethyl-3-Methylimidazolium Iodide Interface. *Electrochem. commun.* **2014**, *46*, 18–21.
121. Lin, L.G.; Wang, Y.; Yan, J.W.; Yuan, Y.Z.; Xiang, J.; Mao, B.W. An in Situ STM Study on the Long-Range Surface Restructuring of Au(111) in a Non-Chloroaluminated Ionic Liquid. *Electrochem. commun.* **2003**, *5*, 995–999.
122. Atkin, R.; Borisenko, N.; Drüscher, M.; Abedin, S.Z.E.; Endres, F.; Hayes, R.; Huber, B.; Roling, B. An in Situ STM/ AFM and Impedance Spectroscopy Study of the Extremely Pure 1-Butyl-1-Methylpyrrolidinium Tris(Pentafluoroethyl)Trifluorophosphate/Au(111) Interface: Potential Dependent Solvation Layers and the Herringbone Reconstruction. *Phys. Chem. Chem. Phys.* **2011**, *13*, 6849–6857.
123. Maurice, V.; Strehblow, H.-H.; Marcus, P. In Situ STM Study of the Initial Stages of Oxidation of Cu(111) in Aqueous Solution. *Surf. Sci.* **2000**, *458*, 185–194.
124. Engelbrekt, C.; Nazmutdinov, R.R.; Zinkicheva, T.T.; Glukhov, D.V.; Yan, J.; Mao, B.; Ulstrup, J.; Zhang, J. Chemistry of Cysteine Assembly on Au(100): Electrochemistry, in Situ STM and Molecular Modeling. *Nanoscale* **2019**, *11*, 17235–17251.
125. Zhao, J.; Gorbatovski, G.; Oll, O.; Anderson, E.; Lust, E. Influence of Water on the Electrochemical Characteristics and Nanostructure of Bi(Hkl) | Ionic Liquid Interface. *Electrochim. Acta* **2022**, *415*, 140263.
126. Nečas, D.; Klapetek, P. Gwyddion: An Open-Source Software for SPM Data Analysis. *Open Physics* **2012**, *10*, 181–188.
127. Tee, E.; Tallo, I.; Kurig, H.; Thomberg, T.; Jänes, A.; Lust, E. Huge Enhancement of Energy Storage Capacity and Power Density of Supercapacitors Based on the Carbon Dioxide Activated Microporous SiC-CDC. *Electrochim. Acta* **2015**, *161*, 364–370.
128. Zhao, J.; Gorbatovski, G.; Oll, O.; Thomberg, T.; Lust, E. Effect of Alkali and Halide Ion Doping on the Energy Storage Characteristics of Ionic Liquid Based Supercapacitors. *Electrochim. Acta* **2019**, *319*, 82–87.
129. Oll, O.; Väärtnõu, M.; Gorbatovski, G.; Zhao, J.; Siimenson, C.; Siinor, L.; Lust, K.; Romann, T.; Pikma, P.; Lust, E. Adsorption of Anions on Bismuth and Cadmium Single Crystal Plane Electrodes from Various Solvents and Ionic Liquid Mixtures. *Electrochim. Acta* **2019**, *319*, 895–908.
130. Väärtnõu, M.; Lust, E. Adsorption of Iodide Ions on Bismuth Single Crystal Planes from Solutions in Ethanol. *Electrochim. Acta* **2001**, *47*, 997–1005.
131. Väärtnõu, M.; Lust, E. Adsorption of Iodide Ions on Bismuth Single Crystal Planes from Solutions in Methanol. *Electrochim. Acta* **1999**, *44*, 2437–2444.
132. Oll, O.; Siimenson, C.; Lust, K.; Gorbatovski, G.; Lust, E. Specific Adsorption from an Ionic Liquid: Impedance Study of Iodide Ion Adsorption from a Pure Halide Ionic Liquid at Bismuth Single Crystal Planes. *Electrochim. Acta* **2017**, *247*, 910–919.
133. Lota, G.; Frackowiak, E. Striking Capacitance of Carbon/Iodide Interface. *Electrochem. commun.* **2009**, *11*, 87–90.
134. Hurwitz, H.D. Direct Determination of the Surface Excess of Specifically Adsorbed Ions on Mercury. *J. Electroanal. Chem.* **1965**, *10*, 35–41.
135. Dutkiewicz, E.; Parsons, R. The Adsorption of Iodide Ion from Aqueous KI + KF of Constant Ionic Strength. *J. Electroanal. Chem.* **1966**, *11*, 100–110.
136. Väärtnõu, M.; Lust, E. Electrical Double Layer and Adsorption of Iodide Ions at the Bi | Acetonitrile Interface. *J. Solid State Electrochem.* **2014**, *18*, 173–180.

137. Väärtnõu, M.; Lust, E. Electrical Double Layer and Adsorption of Iodide Ions at the Bis(ethylene Carbonate) Interface. *J. Solid State Electrochem.* **2017**, *21*, 193–201.
138. Väärtnõu, M.; Lust, E. Electrical Double Layer and Adsorption of Iodide Ions at the Bis(gamma-Butyrolactone) Interface. *J. Electroanal. Chem.* **2014**, *733*, 20–26.
139. Väärtnõu, M.; Lust, E. Electrical Double Layer and Adsorption of Iodide Ions at the Bis(propylene Carbonate) Interface. *J. Electroanal. Chem.* **2012**, *686*, 63–68.
140. Siimenson, C.; Lembinen, M.; Oll, O.; Läll, L.; Tarkanovskaja, M.; Ivaništšev, V.; Siinor, L.; Thomberg, T.; Lust, K.; Lust, E. Electrochemical Investigation of 1-Ethyl-3-Methylimidazolium Bromide and Tetrafluoroborate Mixture at Bi(111) Electrode Interface. *J. Electrochem. Soc.* **2016**, *163*, H723–H730.
141. Siinor, L.; Siimenson, C.; Lust, K.; Lust, E. Mixture of 1-Ethyl-3-Methylimidazolium Tetrafluoroborate and 1-Ethyl-3-Methylimidazolium Iodide: A New Potential High Capacitance Electrolyte for EDLCs. *Electrochem. commun.* **2013**, *35*, 5–7.
142. Siimenson, C.; Siinor, L.; Lust, K.; Lust, E. The Electrochemical Characteristics of the Mixture of 1-Ethyl-3-Methylimidazolium Tetrafluoroborate and 1-Ethyl-3-Methylimidazolium Iodide. *J. Electroanal. Chem.* **2014**, *730*, 59–64.
143. Siimenson, C.; Siinor, L.; Lust, K.; Lust, E. Electrochemical Characterization of Iodide Ions Adsorption Kinetics at Bi(111) Electrode from Three-Component Ionic Liquids Mixtures. *ECS Electrochem. Lett.* **2015**, *4*, H62–H65.
144. Motobayashi, K.; Osawa, M. Potential-Dependent Condensation of Water at the Interface between Ionic Liquid [BMIM][TfSA] and an Au Electrode. *Electrochem. commun.* **2016**, *65*, 14–17.
145. Cui, T.; Lahiri, A.; Carstens, T.; Borisenko, N.; Pulletikurthi, G.; Kuhl, C.; Endres, F. Influence of Water on the Electrified Ionic Liquid/Solid Interface: A Direct Observation of the Transition from a Multilayered Structure to a Double-Layer Structure. *J. Phys. Chem. C* **2016**, *120*, 9341–9349.
146. Feng, G.; Jiang, X.; Qiao, R.; Kornyshev, A.A. Water in Ionic Liquids at Electrified Interfaces: The Anatomy of Electrosorption. *ACS Nano* **2014**, *8*, 11685–11694.
147. Zhang, Y.; Ye, R.; Henkensmeier, D.; Hempelmann, R.; Chen, R. “Water-in-Ionic Liquid” Solutions towards Wide Electrochemical Stability Windows for Aqueous Rechargeable Batteries. *Electrochim. Acta* **2018**, *263*, 47–52.
148. Friedl, J.; Markovits, I.I.E.; Herpich, M.; Feng, G.; Kornyshev, A.A.; Stimming, U. Interface between an Au(111) Surface and an Ionic Liquid: The Influence of Water on the Double-Layer Capacitance. *ChemElectroChem* **2017**, *4*, 216–220.
149. Bi, S.; Wang, R.; Liu, S.; Yan, J.; Mao, B.; Kornyshev, A.A.; Feng, G. Minimizing the Electrosorption of Water from Humid Ionic Liquids on Electrodes. *Nat. Commun.* **2018**, *9*, 5222.
150. Kolb, D.M. Reconstruction Phenomena at Metal-Electrolyte Interfaces. *Prog. Surf. Sci.* **1996**, *51*, 109–173.
151. Voroshylova, I.V.; Ers, H.; Koverga, V.; Docampo-Álvarez, B.; Pikma, P.; Ivaništšev, V.B.; Cordeiro, M.N.D.S. Ionic Liquid–Metal Interface: The Origins of Capacitance Peaks. *Electrochim. Acta* **2021**, *379*, 138148.
152. Magnussen, O.M.; Groß, A. Toward an Atomic-Scale Understanding of Electrochemical Interface Structure and Dynamics. *J. Am. Chem. Soc.* **2019**, *141*, 4777–4790.

153. Bandarenka, A.S. Exploring the Interfaces between Metal Electrodes and Aqueous Electrolytes with Electrochemical Impedance Spectroscopy. *Analyst* **2013**, *138*, 5540–5554.
154. Simon, P.; Gogotsi, Y. Capacitive Energy Storage in Nanostructured Carbon–Electrolyte Systems. *Acc. Chem. Res.* **2013**, *46*, 1094–1103.
155. Thomberg, T.; Tooming, T.; Romann, T.; Palm, R.; Jänes, A.; Lust, E. High Power Density Supercapacitors Based on the Carbon Dioxide Activated D-Glucose Derived Carbon Electrodes and Acetonitrile Electrolyte. *J. Electrochem. Soc.* **2013**, *160*, A1834–A1841.
156. Dyatkin, B.; Mamontov, E.; Cook, K.M.; Gogotsi, Y. Capacitance, Charge Dynamics, and Electrolyte–Surface Interactions in Functionalized Carbide-Derived Carbon Electrodes. *Prog. Nat. Sci.* **2015**, *25*, 631–641.
157. Larcher, D.; Tarascon, J.-M. Towards Greener and More Sustainable Batteries for Electrical Energy Storage. *Nature Chem.* **2015**, *7*, 19–29.
158. Li, Q.; Bjerrum, N.J. Aluminum as Anode for Energy Storage and Conversion: A Review. *Journal of Power Sources* **2002**, *110*, 1–10.
159. Elia, G.A.; Marquardt, K.; Hoeppe, K.; Fantini, S.; Lin, R.; Knipping, E.; Peters, W.; Drillet, J.-F.; Passerini, S.; Hahn, R. An Overview and Future Perspectives of Aluminum Batteries. *Adv. Mater.* **2016**, *28*, 7564–7579.
160. Lin, M.-C.; Gong, M.; Lu, B.; Wu, Y.; Wang, D.-Y.; Guan, M.; Angell, M.; Chen, C.; Yang, J.; Hwang, B.-J.; et al. An Ultrafast Rechargeable Aluminium-Ion Battery. *Nature* **2015**, *520*, 324–328.
161. Liu, Z.; Pulletikurthi, G.; Endres, F. A Prussian Blue/Zinc Secondary Battery with a Bio-Ionic Liquid–Water Mixture as Electrolyte. *ACS Appl. Mater. Interfaces* **2016**, *8*, 12158–12164.
162. Lahiri, A.; Borisenko, N.; Olschewski, M.; Pulletikurthi, G.; Endres, F. Anomalous Electroless Deposition of Less Noble Metals on Cu in Ionic Liquids and Its Application towards Battery Electrodes. *Faraday Discuss.* **2017**, *206*, 339–351.
163. Hasa, I.; Passerini, S.; Hassoun, J. A Rechargeable Sodium-Ion Battery Using a Nanostructured Sb–C Anode and P2-Type Layered Na_{0.6}Ni_{0.22}Fe_{0.11}Mn_{0.66}O₂ Cathode. *RSC Adv.* **2015**, *5*, 48928–48934.
164. Hasa, I.; Passerini, S.; Hassoun, J. Characteristics of an Ionic Liquid Electrolyte for Sodium-Ion Batteries. *J. Power Sources* **2016**, *303*, 203–207.
165. Yabuuchi, N.; Kubota, K.; Dahbi, M.; Komaba, S. Research Development on Sodium-Ion Batteries. *Chem. Rev.* **2014**, *114*, 11636–11682.
166. Ren, X.; Wu, Y. A Low-Overpotential Potassium–Oxygen Battery Based on Potassium Superoxide. *J. Am. Chem. Soc.* **2013**, *135*, 2923–2926.
167. Shatla, A.S.; Abd-El-Latif, A.A.; Ayata, S.; Demir, D.; Baltruschat, H. Iodide Adsorption at Au(111) Electrode in Non-Aqueous Electrolyte: AC-Voltammetry and EIS Studies. *Electrochim. Acta* **2019**, 135556.
168. Zhang, Q.; Liu, X.; Yin, L.; Chen, P.; Wang, Y.; Yan, T. Electrochemical Impedance Spectroscopy on the Capacitance of Ionic Liquid–Acetonitrile Electrolytes. *Electrochim. Acta* **2018**, *270*, 352–362.
169. Romann, T.; Oll, O.; Pikma, P.; Lust, E. Abnormal Infrared Effects on Bismuth Thin Film–EMImBF₄ Ionic Liquid Interface. *Electrochem. commun.* **2012**, *23*, 118–121.
170. Gorbatovski, G.; Oll, O.; Kasuk, H.; Pikma, P.; Lust, E. In Situ Scanning Tunneling Microscopy Study of Bipyridine Adsorption at Semi-Metallic Sb(111) Plane. *Electrochem. commun.* **2019**, *105*, 106500.

171. Lust, E.; Jänes, A.; Lust, K.; Väärtnõu, M. Electric Double Layer Structure and Adsorption of Cyclohexanol on Single Crystal Cadmium, Antimony and Bismuth Electrodes. *Electrochim. Acta* **1997**, *42*, 771–783.
172. Zhang, Y.; Liu, S.; Ji, Y.; Ma, J.; Yu, H. Emerging Nonaqueous Aluminum-Ion Batteries: Challenges, Status, and Perspectives. *Adv. Mater.* **2018**, *30*, 1706310.
173. Wang, H.; Gu, S.; Bai, Y.; Chen, S.; Wu, F.; Wu, C. High-Voltage and Non-corrosive Ionic Liquid Electrolyte Used in Rechargeable Aluminum Battery. *ACS Appl. Mater. Interfaces* **2016**, *8*, 27444–27448.

9. SUMMARY IN ESTONIAN

Ioosetel vedelikel põhinevate elektrolüütide elektrokeemilised omadused Bi(hkl) ja mikro-mesopoorsetel süsinik elektroodidel

Tänapäeva tehnoloogias ja teaduses on olulisel kohal moodsad energia muundamise ja salvestamise seadmed. Ioosned vedelikud omavad olulist tehnoloogilist potentsiaali antud seadmetes tänu nende kõrgele keemilisele stabiilsusele, laiale variatsioonile ning rakendatavusele nii elektrolüüdi kui solvendina. Selleks, et disainida efektiivsemaid ja kõrgema erieneergiaga energiasalvesteid on oluline mõista mehhanisme, mis mõjutavad energia salvestamist ioonseid vedelike rakendavates süsteemides, nagu näiteks super- ja hübriidkondensaatorites. Elektrilise kaksikkihi (EKK) tekke ja dünaamika ning lisandite mõju, nagu näiteks halogeniid ja leelismetalli ioonid, vesi ja orgaanilised solvendid, uurimine võimaldab meil teadlikult disainida paremaid elektrokeemilisi seadmeid. Antud töös uuriti nii mudelektrood-süsteeme, et näidata lisandite mõju EKK tekkele vismuti monokristalli eri tahkudel, kui ka superkondensaatori test-rakke, et kontrollida, kuivõrd fundamentaaluuuringutest saadavad teadmised on rakendatavad ka reaalsetes seadmetes.

Antud töös kasutati elektrokeemilise impedantspektroskoopia, skaneeriva tunnelmikroskoopia ja alalisvoolu elektrokeemilisi meetodeid, et iseloomustada erinevate ioonsete vedelike mahtvuslikke, takistuslisi ja adsorptsioonilisi omadusi vismuti monokristallide ja mikro-mesopoorse süsinikmaterjali piirpinnal. Lisaks vaadeldi erinevate pindaktiivsete lisandite mõju vastavate süsteemide omadustele. Tulemustest nähtub, et kõige olulisemat mõju vastavate süsteemide elektrood | elektrolüüt piirpinnale omavad ioonse vedeliku anioonid ning lahustunud molekulid mis omavad tugevat vastastikmõju anioonidega. Näidati, et anioonide varieerimine muudab oluliselt piirpinna mahtuvust, eriti polariseeritavamate anioonide nagu näiteks halogeniid-ioonide puhul. Skaneeriva tunnelmikroskoopia tulemustest võib järeldada, et mahtuvuse muutus on tingitud kõrgelt struktureeritud tiheda adsorptsioonilise kihi tekkest vismuti monokristallide piirpinnale. Samuti uuriti vee kui lisandi mõju Bi | ioonne vedelik süsteemile. Kõrge hügrooskoopsuse tõttu on väike vee lisand levinud paljudes uuritavates süsteemides, ning vastava mõju hindamine omab olulist väärtust rakendustele. Ka siin leiti, et kõige olulisem muutus puudutab ioonse vedeliku anioone, mis veemolekulide olemasolu korral on võimelised moodustama hüdrateeritud komplekse, mis omavad olulist mõju vismutielektroodi mahtvuslikele omadustele, eriti positiivse pinnalaengu korral. Samuti on vee-lisandil arvestatav mõju takistuslikele parameetritele, kuna vesi on elektrokeemiliselt ioonsetest vedelikest vähem stabiilsem.

Ioosnete lisandite mõju superkondensaatorites uurimiseks võrreldi puhas ioonset vedelikku kui elektrolüüti sisaldavat süsteemi ning lisati nendele nii halogeniid kui ka leelismetalli ioone. Vastavad lisandid olid kasutusel abrosbee-

rituna mikro-mesopoores süsinikmaterjalis, milles oluline osa poorsusest on suurematele ioonse vedeliku anioonidele ja kationidele suletud. Seega võis eeldada, et väikesemad lisandi-ioonid on peamiselt kontsentreerunud materjali mikropooridesse. Näidati, et kuigi leelis-metallide ionid ei oma olulist mõju superkondensaatori mahtvusele, siis halogeniidioonid aitavad parendada süsteemi elektrokeemilisi omadusi olulisel määral. Seega on ka antud süsteemides aniooni mõju elektrokeemilistele omadustele ja EKK tekkele määrava tähtsusega. Täpsem impedants-spektrite analüüs võimaldas lahtutada vastava mõju nii mahtvuslikuks kui ka laengu-ülekande komponentideks, aidates mõista halogeniidioonide mõju hübriidkondensaatorile.

10. ACKNOWLEDGEMENTS

Having joined in the University of Tartu, Institute of Chemistry for my doctoral study is a great adventure. I am grateful to spend these challenging but joyous years here, lucky to meet and work together with so many great and lovely people during my studies.

First and foremost, I would like to sincerely thank my supervisors, Prof. Enn Lust and Dr. Ove Oll. Starting from Enn, offering me an opportunity to join this group, his kind support and encouragement make me feel at home. His rich knowledge and experience can always point out a general direction to innovate my experimental projects. His attitude and passion for work make me understand what a real scientist should be. Whether at late hours on weekdays or weekends, he is always in the office. As a result, he acted as a great example to inspire me to like spending more time in Chemicum. Then, I would like to express my special thanks to Ove, who helped me adapt to the lab work quickly when I first came to Tartu. Throughout the adventure in experiments, he was always guiding and teaching me to understand how things work. He is also a role model because his intelligence and great ideas can always help me clear the obstacles when needed. I feel so lucky to have met him and worked with him over the years, and I wouldn't be here today without his help. Thank you!

Without my lovely colleagues, the years spent in Estonia would not have been so wonderful and interesting. I want to start by thanking Carolin Siimenson and Liis Siinor, whom I first met in our group when I came to Tartu. They helped me quickly adapt to life and study in Tartu. They invited me to join in many interesting activities that made my life in Tartu much more enjoyable, despite being thousands of miles away from home. We shared a lot of wonderful memorable moments. And I want to thank Ove Korjus, Peeter Valk, and Patrick Teppor. They helped me a lot, including the Estonian language translations and the technical problems (here, I also want to thank Rait Kanarbik for the technical support). I felt so lucky to share the same office with them during the years. Then I would like to thank Georg Gorbatovski and Silvester Jürjo, with them we shared many great moments in both work discussions and other activities. Then, many thanks to Piret Pikma and Thomas Thomberg, Piret for funding a part of my doctoral study, and Thomas for his professional guidance and help in the supercapacitor field. I also thank Karmen Lust for helping to review the thesis. Finally, big thanks are for all the great people that I worked with in the same group: Jaak Nerut, Heili Kasuk, Martin Maide, Meelis Härmas, Rasmus Palm, Vladislav Ivaništšev, Alar Jänes, Alar Heinsaar, Gunnar Nurk, Indrek Kivi, Jaanus Kruusma, Jaanus Eskusson, Heigo Ers, Rutha Jäger, Riinu Härmas, Maarja Paalo, Huy Qui Vinh Nguyen, Sara Paydar, Eva-Liisa Tooming, Silver Sepp, Miriam Koppel, Kenneth Tuul, Annabel Olgo, Mart Väärt-nõu, Anu Adamson, etc. I spent many nice moments with them in Chemicum during the years. Beyond the lab circle, I also want to thank all the friends I met in Estonia for an unforgettable time abroad.

I want to thank my family sincerely for their ongoing support and encouragement, always giving me the motivation to move forward. Many thanks also to my friends who are always there for me even though we were far apart.

Finally, I am grateful for the funding to support during my doctoral studies: Estonian Ministry of Education and Research (projects no. IUT 20-13, PRG676, PSG249, PUT1033, and PUT1107), the EU through the European Regional Development Fund Centers of Excellence, TK141 (2014-2020.4.01.15-0011), Graduate School of Functional Materials and Technologies under the project at University of Tartu and Dora Plus short-term mobility. Also, I would like to thank the China Scholarship Council (201706890009).

11. PUBLICATIONS

CURRICULUM VITAE

Name: Jinfeng Zhao
Date of birth: April 24, 1990
Citizenship: People's Republic of China
Contact: Institute of Chemistry, University of Tartu
Ravila 14A, 50411, Tartu, Estonia
E-mail: jinfeng.zhao@ut.ee

Education:

2017– University of Tartu, Institute of Chemistry – *Ph.D.* student
2014–2017 Shanghai University, Institute of Chemistry – *M.Sc.* in
Chemistry
2010–2014 Anhui Normal University, Institute of Chemistry – *B.Sc.* in
Chemistry

Scientific organizations:

2018– Member of the International Society of Electrochemistry

List of publications:

1. **J. Zhao**, G. Gorbatovski, O. Oll, T. Thomberg, E. Lust, Effect of alkali and halide ion doping on the energy storage characteristics of ionic liquid based supercapacitors, *Electrochimica Acta*. 319 (2019) 82–87.
2. O. Oll, M. Väärtnõu, G. Gorbatovski, **J. Zhao**, C. Siimenson, L. Siinor, K. Lust, T. Romann, P. Pikma, E. Lust, Adsorption of anions on bismuth and cadmium single crystal plane electrodes from various solvents and ionic liquid mixtures, *Electrochimica Acta*. 319 (2019) 895–908.
3. **J. Zhao**, G. Gorbatovski, O. Oll, E. Anderson, E. Lust, Influence of water on the electrochemical characteristics and nanostructure of Bi(*hkl*) | ionic liquid interface, *Electrochimica Acta*. 415 (2022) 140263.
4. S. Jürjo, O. Oll, P. Paiste, M. Külaviir, **J. Zhao**, E. Lust, Electrochemical co-reduction of praseodymium and bismuth from 1-butyl-1-methylpyrrolidinium bis(fluorosulfonyl)imide ionic liquid, *Electrochemistry Communications* 138 (2022) 107285.
5. **J. Zhao**, G. Gorbatovski, O. Oll, T. Thomberg, E. Lust, Analysis of impedance: the distribution of capacitance in halide ion treated supercapacitors (Under review).

International conference presentations:

1. **J. Zhao**, O. Oll, G. Gorbatovski and E. Lust, Exploring the Interfacial Behavior of Aluminum Electrode in Ionic Liquids: An Impedance Study, 71st annual Meeting of the International Society of Electrochemistry (online), Belgrade, Serbia, 30th August–4th September, 2020.

2. **J. Zhao**, O. Oll, G. Gorbatovski, E. Anderson and E. Lust, Influence of Water on the Interface between Hydrophilic Ionic Liquid and Single Crystal Bismuth Electrodes, Electrochemical Conference on Energy and the Environment: Bioelectrochemistry and Energy Storage (ECEE 2019), Glasgow, Scotland, 21–26th July, 2019.
3. **J. Zhao**, O. Oll, G. Gorbatovski, T. Thomberg and E. Lust, Efficiency and Capacitive Behavior of Supercapacitors Based on Carbon Electrodes Containing Ionic Liquids with Halide and Alkali Ions, 7th Baltic Electrochemistry Conference, Tartu, Estonia, 4–7th November, 2018.
4. **J. Zhao**, O. Oll, E. Anderson, G. Gorbatovski and E. Lust, Influence of Water Additive on the Specific Adsorption from an Ionic Liquid at Single Crystal Bismuth Electrodes, 69th Annual ISE Meeting of International Society of Electrochemistry, Bologna, Italy. 2–7th September, 2018.

ELULOOKIRJELDUS

Nimi: Jinfeng Zhao
Sünniaeg: 24. aprill 1990
Kodakondsus: Hiina Rahvavabariik
Kontakt: keemia instituut, Tartu Ülikool
Ravila 14A, 50411, Tartu, Eesti
E-post: jinfeng.zhao@ut.ee

Haridus:
2017– Tartu Ülikool, keemia instituut – doktorant
2014–2017 Shanghai Ülikool, keemia instituut – *M.Sc.* keemia erialal
2010–2014 Anhui Pedagoogiline Ülikool, keemia instituut – *B.Sc.*
keemia erialal

Teadusorganisatsioonid:

2018– Rahvusvahelise elektrokeemiaühingu liige

Teaduspublikatsioonid:

1. **J. Zhao**, G. Gorbatovski, O. Oll, T. Thomberg, E. Lust, Effect of alkali and halide ion doping on the energy storage characteristics of ionic liquid based supercapacitors, *Electrochimica Acta*. 319 (2019) 82–87.
2. O. Oll, M. Väärtnõu, G. Gorbatovski, **J. Zhao**, C. Siimenson, L. Siinor, K. Lust, T. Romann, P. Pikma, E. Lust, Adsorption of anions on bismuth and cadmium single crystal plane electrodes from various solvents and ionic liquid mixtures, *Electrochimica Acta*. 319 (2019) 895–908.
3. **J. Zhao**, G. Gorbatovski, O. Oll, E. Anderson, E. Lust, Influence of water on the electrochemical characteristics and nanostructure of Bi(*hkl*) | ionic liquid interface, *Electrochimica Acta*. 415 (2022) 140263.
4. S. Jürjo, O. Oll, P. Paiste, M. Külaviir, **J. Zhao**, E. Lust, Electrochemical co-reduction of praseodymium and bismuth from 1-butyl-1-methylpyrrolidinium bis(fluorosulfonyl)imide ionic liquid, *Electrochemistry Communications* 138 (2022) 107285.
5. **J. Zhao**, G. Gorbatovski, O. Oll, T. Thomberg, E. Lust, Analysis of impedance: the distribution of capacitance in halide ion treated supercapacitors (avaldamisel).

Rahvusvahelised konverentsiettekanded:

1. **J. Zhao**, O. Oll, G. Gorbatovski and E. Lust, Exploring the Interfacial Behavior of Aluminum Electrode in Ionic Liquids: An Impedance Study, 71st annual Meeting of the International Society of Electrochemistry (online), Belgrade, Serbia, 30th August–4th September, 2020.
2. **J. Zhao**, O. Oll, G. Gorbatovski, E. Anderson and E. Lust, Influence of Water on the Interface between Hydrophilic Ionic Liquid and Single Crystal

Bismuth Electrodes, Electrochemical Conference on Energy and the Environment: Bioelectrochemistry and Energy Storage (ECEE 2019), Glasgow, Scotland, 21–26th July, 2019.

3. **J. Zhao**, O. Oll, G. Gorbatovski, T. Thomberg and E. Lust, Efficiency and Capacitive Behavior of Supercapacitors Based on Carbon Electrodes Containing Ionic Liquids with Halide and Alkali Ions, 7th Baltic Electrochemistry Conference, Tartu, Estonia, 4–7th November, 2018.
4. **J. Zhao**, O. Oll, E. Anderson, G. Gorbatovski and E. Lust, Influence of Water Additive on the Specific Adsorption from an Ionic Liquid at Single Crystal Bismuth Electrodes, 69th Annual ISE Meeting of International Society of Electrochemistry, Bologna, Italy. 2–7th September, 2018.

DISSERTATIONES CHIMICAE UNIVERSITATIS TARTUENSIS

1. **Toomas Tamm.** Quantum-chemical simulation of solvent effects. Tartu, 1993, 110 p.
2. **Peeter Burk.** Theoretical study of gas-phase acid-base equilibria. Tartu, 1994, 96 p.
3. **Victor Lobanov.** Quantitative structure-property relationships in large descriptor spaces. Tartu, 1995, 135 p.
4. **Vahur Mäemets.** The ^{17}O and ^1H nuclear magnetic resonance study of H_2O in individual solvents and its charged clusters in aqueous solutions of electrolytes. Tartu, 1997, 140 p.
5. **Andrus Metsala.** Microcanonical rate constant in nonequilibrium distribution of vibrational energy and in restricted intramolecular vibrational energy redistribution on the basis of Slater's theory of unimolecular reactions. Tartu, 1997, 150 p.
6. **Uko Maran.** Quantum-mechanical study of potential energy surfaces in different environments. Tartu, 1997, 137 p.
7. **Alar Jänes.** Adsorption of organic compounds on antimony, bismuth and cadmium electrodes. Tartu, 1998, 219 p.
8. **Kaido Tammeveski.** Oxygen electroreduction on thin platinum films and the electrochemical detection of superoxide anion. Tartu, 1998, 139 p.
9. **Ivo Leito.** Studies of Brønsted acid-base equilibria in water and non-aqueous media. Tartu, 1998, 101 p.
10. **Jaan Leis.** Conformational dynamics and equilibria in amides. Tartu, 1998, 131 p.
11. **Toonika Rinke.** The modelling of amperometric biosensors based on oxidoreductases. Tartu, 2000, 108 p.
12. **Dmitri Panov.** Partially solvated Grignard reagents. Tartu, 2000, 64 p.
13. **Kaja Orupõld.** Treatment and analysis of phenolic wastewater with microorganisms. Tartu, 2000, 123 p.
14. **Jüri Ivask.** Ion Chromatographic determination of major anions and cations in polar ice core. Tartu, 2000, 85 p.
15. **Lauri Vares.** Stereoselective Synthesis of Tetrahydrofuran and Tetrahydropyran Derivatives by Use of Asymmetric Horner-Wadsworth-Emmons and Ring Closure Reactions. Tartu, 2000, 184 p.
16. **Martin Lepiku.** Kinetic aspects of dopamine D_2 receptor interactions with specific ligands. Tartu, 2000, 81 p.
17. **Katrin Sak.** Some aspects of ligand specificity of P_2Y receptors. Tartu, 2000, 106 p.
18. **Vello Pällin.** The role of solvation in the formation of iotritch complexes. Tartu, 2001, 95 p.
19. **Katrin Kollist.** Interactions between polycyclic aromatic compounds and humic substances. Tartu, 2001, 93 p.

20. **Ivar Koppel.** Quantum chemical study of acidity of strong and superstrong Brønsted acids. Tartu, 2001, 104 p.
21. **Viljar Pihl.** The study of the substituent and solvent effects on the acidity of OH and CH acids. Tartu, 2001, 132 p.
22. **Natalia Palm.** Specification of the minimum, sufficient and significant set of descriptors for general description of solvent effects. Tartu, 2001, 134 p.
23. **Sulev Sild.** QSPR/QSAR approaches for complex molecular systems. Tartu, 2001, 134 p.
24. **Ruslan Petrukhin.** Industrial applications of the quantitative structure-property relationships. Tartu, 2001, 162 p.
25. **Boris V. Rogovoy.** Synthesis of (benzotriazolyl)carboximidamides and their application in relations with *N*- and *S*-nucleophiles. Tartu, 2002, 84 p.
26. **Koit Herodes.** Solvent effects on UV-vis absorption spectra of some solvatochromic substances in binary solvent mixtures: the preferential solvation model. Tartu, 2002, 102 p.
27. **Anti Perkson.** Synthesis and characterisation of nanostructured carbon. Tartu, 2002, 152 p.
28. **Ivari Kaljurand.** Self-consistent acidity scales of neutral and cationic Brønsted acids in acetonitrile and tetrahydrofuran. Tartu, 2003, 108 p.
29. **Karmen Lust.** Adsorption of anions on bismuth single crystal electrodes. Tartu, 2003, 128 p.
30. **Mare Piirsalu.** Substituent, temperature and solvent effects on the alkaline hydrolysis of substituted phenyl and alkyl esters of benzoic acid. Tartu, 2003, 156 p.
31. **Meeri Sassian.** Reactions of partially solvated Grignard reagents. Tartu, 2003, 78 p.
32. **Tarmo Tamm.** Quantum chemical modelling of polypyrrole. Tartu, 2003. 100 p.
33. **Erik Teinmaa.** The environmental fate of the particulate matter and organic pollutants from an oil shale power plant. Tartu, 2003. 102 p.
34. **Jaana Tammiku-Taul.** Quantum chemical study of the properties of Grignard reagents. Tartu, 2003. 120 p.
35. **Andre Lomaka.** Biomedical applications of predictive computational chemistry. Tartu, 2003. 132 p.
36. **Kostyantyn Kirichenko.** Benzotriazole – Mediated Carbon–Carbon Bond Formation. Tartu, 2003. 132 p.
37. **Gunnar Nurk.** Adsorption kinetics of some organic compounds on bismuth single crystal electrodes. Tartu, 2003, 170 p.
38. **Mati Arulepp.** Electrochemical characteristics of porous carbon materials and electrical double layer capacitors. Tartu, 2003, 196 p.
39. **Dan Cornel Fara.** QSPR modeling of complexation and distribution of organic compounds. Tartu, 2004, 126 p.
40. **Riina Mahlapuu.** Signalling of galanin and amyloid precursor protein through adenylate cyclase. Tartu, 2004, 124 p.

41. **Mihkel Kerikmäe.** Some luminescent materials for dosimetric applications and physical research. Tartu, 2004, 143 p.
42. **Jaanus Kruusma.** Determination of some important trace metal ions in human blood. Tartu, 2004, 115 p.
43. **Urmas Johanson.** Investigations of the electrochemical properties of polypyrrole modified electrodes. Tartu, 2004, 91 p.
44. **Kaido Sillar.** Computational study of the acid sites in zeolite ZSM-5. Tartu, 2004, 80 p.
45. **Aldo Oras.** Kinetic aspects of dATP α S interaction with P2Y₁ receptor. Tartu, 2004, 75 p.
46. **Erik Mölder.** Measurement of the oxygen mass transfer through the air-water interface. Tartu, 2005, 73 p.
47. **Thomas Thomborg.** The kinetics of electroreduction of peroxodisulfate anion on cadmium (0001) single crystal electrode. Tartu, 2005, 95 p.
48. **Olavi Loog.** Aspects of condensations of carbonyl compounds and their imine analogues. Tartu, 2005, 83 p.
49. **Siim Salmar.** Effect of ultrasound on ester hydrolysis in aqueous ethanol. Tartu, 2006, 73 p.
50. **Ain Uustare.** Modulation of signal transduction of heptahelical receptors by other receptors and G proteins. Tartu, 2006, 121 p.
51. **Sergei Yurchenko.** Determination of some carcinogenic contaminants in food. Tartu, 2006, 143 p.
52. **Kaido Tämm.** QSPR modeling of some properties of organic compounds. Tartu, 2006, 67 p.
53. **Olga Tšubrik.** New methods in the synthesis of multisubstituted hydrazines. Tartu, 2006, 183 p.
54. **Lilli Sooväli.** Spectrophotometric measurements and their uncertainty in chemical analysis and dissociation constant measurements. Tartu, 2006, 125 p.
55. **Eve Koort.** Uncertainty estimation of potentiometrically measured pH and pK_a values. Tartu, 2006, 139 p.
56. **Sergei Kopanchuk.** Regulation of ligand binding to melanocortin receptor subtypes. Tartu, 2006, 119 p.
57. **Silvar Kallip.** Surface structure of some bismuth and antimony single crystal electrodes. Tartu, 2006, 107 p.
58. **Kristjan Saal.** Surface silanization and its application in biomolecule coupling. Tartu, 2006, 77 p.
59. **Tanel Tätte.** High viscosity Sn(OBu)₄ oligomeric concentrates and their applications in technology. Tartu, 2006, 91 p.
60. **Dimitar Atanasov Dobchev.** Robust QSAR methods for the prediction of properties from molecular structure. Tartu, 2006, 118 p.
61. **Hannes Hagu.** Impact of ultrasound on hydrophobic interactions in solutions. Tartu, 2007, 81 p.
62. **Rutha Jäger.** Electroreduction of peroxodisulfate anion on bismuth electrodes. Tartu, 2007, 142 p.

63. **Kaido Viht.** Immobilizable bisubstrate-analogue inhibitors of basophilic protein kinases: development and application in biosensors. Tartu, 2007, 88 p.
64. **Eva-Ingrid Rõõm.** Acid-base equilibria in nonpolar media. Tartu, 2007, 156 p.
65. **Sven Tamp.** DFT study of the cesium cation containing complexes relevant to the cesium cation binding by the humic acids. Tartu, 2007, 102 p.
66. **Jaak Nerut.** Electroreduction of hexacyanoferrate(III) anion on Cadmium (0001) single crystal electrode. Tartu, 2007, 180 p.
67. **Lauri Jalukse.** Measurement uncertainty estimation in amperometric dissolved oxygen concentration measurement. Tartu, 2007, 112 p.
68. **Aime Lust.** Charge state of dopants and ordered clusters formation in CaF₂:Mn and CaF₂:Eu luminophors. Tartu, 2007, 100 p.
69. **Iiris Kahn.** Quantitative Structure-Activity Relationships of environmentally relevant properties. Tartu, 2007, 98 p.
70. **Mari Reinik.** Nitrates, nitrites, N-nitrosamines and polycyclic aromatic hydrocarbons in food: analytical methods, occurrence and dietary intake. Tartu, 2007, 172 p.
71. **Heili Kasuk.** Thermodynamic parameters and adsorption kinetics of organic compounds forming the compact adsorption layer at Bi single crystal electrodes. Tartu, 2007, 212 p.
72. **Erki Enkvist.** Synthesis of adenosine-peptide conjugates for biological applications. Tartu, 2007, 114 p.
73. **Svetoslav Hristov Slavov.** Biomedical applications of the QSAR approach. Tartu, 2007, 146 p.
74. **Eneli Härk.** Electroreduction of complex cations on electrochemically polished Bi(*hkl*) single crystal electrodes. Tartu, 2008, 158 p.
75. **Priit Möller.** Electrochemical characteristics of some cathodes for medium temperature solid oxide fuel cells, synthesized by solid state reaction technique. Tartu, 2008, 90 p.
76. **Signe Viggor.** Impact of biochemical parameters of genetically different pseudomonads at the degradation of phenolic compounds. Tartu, 2008, 122 p.
77. **Ave Sarapuu.** Electrochemical reduction of oxygen on quinone-modified carbon electrodes and on thin films of platinum and gold. Tartu, 2008, 134 p.
78. **Agnes Kütt.** Studies of acid-base equilibria in non-aqueous media. Tartu, 2008, 198 p.
79. **Rouvim Kadis.** Evaluation of measurement uncertainty in analytical chemistry: related concepts and some points of misinterpretation. Tartu, 2008, 118 p.
80. **Valter Reedo.** Elaboration of IVB group metal oxide structures and their possible applications. Tartu, 2008, 98 p.
81. **Aleksei Kuznetsov.** Allosteric effects in reactions catalyzed by the cAMP-dependent protein kinase catalytic subunit. Tartu, 2009, 133 p.

82. **Aleksei Bredihhin.** Use of mono- and polyanions in the synthesis of multisubstituted hydrazine derivatives. Tartu, 2009, 105 p.
83. **Anu Ploom.** Quantitative structure-reactivity analysis in organosilicon chemistry. Tartu, 2009, 99 p.
84. **Argo Vonk.** Determination of adenosine A_{2A}- and dopamine D₁ receptor-specific modulation of adenylate cyclase activity in rat striatum. Tartu, 2009, 129 p.
85. **Indrek Kivi.** Synthesis and electrochemical characterization of porous cathode materials for intermediate temperature solid oxide fuel cells. Tartu, 2009, 177 p.
86. **Jaanus Eskusson.** Synthesis and characterisation of diamond-like carbon thin films prepared by pulsed laser deposition method. Tartu, 2009, 117 p.
87. **Marko Lätt.** Carbide derived microporous carbon and electrical double layer capacitors. Tartu, 2009, 107 p.
88. **Vladimir Stepanov.** Slow conformational changes in dopamine transporter interaction with its ligands. Tartu, 2009, 103 p.
89. **Aleksander Trummal.** Computational Study of Structural and Solvent Effects on Acidities of Some Brønsted Acids. Tartu, 2009, 103 p.
90. **Eerold Vellemäe.** Applications of mischmetal in organic synthesis. Tartu, 2009, 93 p.
91. **Sven Parkel.** Ligand binding to 5-HT_{1A} receptors and its regulation by Mg²⁺ and Mn²⁺. Tartu, 2010, 99 p.
92. **Signe Vahur.** Expanding the possibilities of ATR-FT-IR spectroscopy in determination of inorganic pigments. Tartu, 2010, 184 p.
93. **Tavo Romann.** Preparation and surface modification of bismuth thin film, porous, and microelectrodes. Tartu, 2010, 155 p.
94. **Nadežda Aleksejeva.** Electrocatalytic reduction of oxygen on carbon nanotube-based nanocomposite materials. Tartu, 2010, 147 p.
95. **Marko Kullapere.** Electrochemical properties of glassy carbon, nickel and gold electrodes modified with aryl groups. Tartu, 2010, 233 p.
96. **Liis Siinor.** Adsorption kinetics of ions at Bi single crystal planes from aqueous electrolyte solutions and room-temperature ionic liquids. Tartu, 2010, 101 p.
97. **Angela Vaasa.** Development of fluorescence-based kinetic and binding assays for characterization of protein kinases and their inhibitors. Tartu 2010, 101 p.
98. **Indrek Tulp.** Multivariate analysis of chemical and biological properties. Tartu 2010, 105 p.
99. **Aare Selberg.** Evaluation of environmental quality in Northern Estonia by the analysis of leachate. Tartu 2010, 117 p.
100. **Darja Lavõgina.** Development of protein kinase inhibitors based on adenosine analogue-oligoarginine conjugates. Tartu 2010, 248 p.
101. **Laura Herm.** Biochemistry of dopamine D₂ receptors and its association with motivated behaviour. Tartu 2010, 156 p.

102. **Terje Raudsepp.** Influence of dopant anions on the electrochemical properties of polypyrrole films. Tartu 2010, 112 p.
103. **Margus Marandi.** Electroformation of Polypyrrole Films: *In-situ* AFM and STM Study. Tartu 2011, 116 p.
104. **Kairi Kivirand.** Diamine oxidase-based biosensors: construction and working principles. Tartu, 2011, 140 p.
105. **Anneli Kruve.** Matrix effects in liquid-chromatography electrospray mass-spectrometry. Tartu, 2011, 156 p.
106. **Gary Urb.** Assessment of environmental impact of oil shale fly ash from PF and CFB combustion. Tartu, 2011, 108 p.
107. **Nikita Oskolkov.** A novel strategy for peptide-mediated cellular delivery and induction of endosomal escape. Tartu, 2011, 106 p.
108. **Dana Martin.** The QSPR/QSAR approach for the prediction of properties of fullerene derivatives. Tartu, 2011, 98 p.
109. **Säde Viirlaid.** Novel glutathione analogues and their antioxidant activity. Tartu, 2011, 106 p.
110. **Ülis Sõukand.** Simultaneous adsorption of Cd²⁺, Ni²⁺, and Pb²⁺ on peat. Tartu, 2011, 124 p.
111. **Lauri Lipping.** The acidity of strong and superstrong Brønsted acids, an outreach for the “limits of growth”: a quantum chemical study. Tartu, 2011, 124 p.
112. **Heisi Kurig.** Electrical double-layer capacitors based on ionic liquids as electrolytes. Tartu, 2011, 146 p.
113. **Marje Kasari.** Bisubstrate luminescent probes, optical sensors and affinity adsorbents for measurement of active protein kinases in biological samples. Tartu, 2012, 126 p.
114. **Kalev Takkis.** Virtual screening of chemical databases for bioactive molecules. Tartu, 2012, 122 p.
115. **Ksenija Kisseljova.** Synthesis of aza-β³-amino acid containing peptides and kinetic study of their phosphorylation by protein kinase A. Tartu, 2012, 104 p.
116. **Riin Rebane.** Advanced method development strategy for derivatization LC/ESI/MS. Tartu, 2012, 184 p.
117. **Vladislav Ivaništšev.** Double layer structure and adsorption kinetics of ions at metal electrodes in room temperature ionic liquids. Tartu, 2012, 128 p.
118. **Irja Helm.** High accuracy gravimetric Winkler method for determination of dissolved oxygen. Tartu, 2012, 139 p.
119. **Karin Kipper.** Fluoroalcohols as Components of LC-ESI-MS Eluents: Usage and Applications. Tartu, 2012, 164 p.
120. **Arno Ratas.** Energy storage and transfer in dosimetric luminescent materials. Tartu, 2012, 163 p.
121. **Reet Reinart-Okugbeni.** Assay systems for characterisation of subtype-selective binding and functional activity of ligands on dopamine receptors. Tartu, 2012, 159 p.

122. **Lauri Sikk.** Computational study of the Sonogashira cross-coupling reaction. Tartu, 2012, 81 p.
123. **Karita Raudkivi.** Neurochemical studies on inter-individual differences in affect-related behaviour of the laboratory rat. Tartu, 2012, 161 p.
124. **Indrek Saar.** Design of GalR2 subtype specific ligands: their role in depression-like behavior and feeding regulation. Tartu, 2013, 126 p.
125. **Ann Laheäär.** Electrochemical characterization of alkali metal salt based non-aqueous electrolytes for supercapacitors. Tartu, 2013, 127 p.
126. **Kerli Tõnurist.** Influence of electrospun separator materials properties on electrochemical performance of electrical double-layer capacitors. Tartu, 2013, 147 p.
127. **Kaija Põhako-Esko.** Novel organic and inorganic ionogels: preparation and characterization. Tartu, 2013, 124 p.
128. **Ivar Kruusenberg.** Electroreduction of oxygen on carbon nanomaterial-based catalysts. Tartu, 2013, 191 p.
129. **Sander Piiskop.** Kinetic effects of ultrasound in aqueous acetonitrile solutions. Tartu, 2013, 95 p.
130. **Ilona Faustova.** Regulatory role of L-type pyruvate kinase N-terminal domain. Tartu, 2013, 109 p.
131. **Kadi Tamm.** Synthesis and characterization of the micro-mesoporous anode materials and testing of the medium temperature solid oxide fuel cell single cells. Tartu, 2013, 138 p.
132. **Iva Bozhidarova Stoyanova-Slavova.** Validation of QSAR/QSPR for regulatory purposes. Tartu, 2013, 109 p.
133. **Vitali Grozovski.** Adsorption of organic molecules at single crystal electrodes studied by *in situ* STM method. Tartu, 2014, 146 p.
134. **Santa Veikšina.** Development of assay systems for characterisation of ligand binding properties to melanocortin 4 receptors. Tartu, 2014, 151 p.
135. **Jüri Liiv.** PVDF (polyvinylidene difluoride) as material for active element of twisting-ball displays. Tartu, 2014, 111 p.
136. **Kersti Vaarmets.** Electrochemical and physical characterization of pristine and activated molybdenum carbide-derived carbon electrodes for the oxygen electroreduction reaction. Tartu, 2014, 131 p.
137. **Lauri Tõntson.** Regulation of G-protein subtypes by receptors, guanine nucleotides and Mn²⁺. Tartu, 2014, 105 p.
138. **Aiko Adamson.** Properties of amine-boranes and phosphorus analogues in the gas phase. Tartu, 2014, 78 p.
139. **Elo Kibena.** Electrochemical grafting of glassy carbon, gold, highly oriented pyrolytic graphite and chemical vapour deposition-grown graphene electrodes by diazonium reduction method. Tartu, 2014, 184 p.
140. **Teemu Näykki.** Novel Tools for Water Quality Monitoring – From Field to Laboratory. Tartu, 2014, 202 p.
141. **Karl Kaupmees.** Acidity and basicity in non-aqueous media: importance of solvent properties and purity. Tartu, 2014, 128 p.

142. **Oleg Lebedev.** Hydrazine polyanions: different strategies in the synthesis of heterocycles. Tartu, 2015, 118 p.
143. **Geven Piir.** Environmental risk assessment of chemicals using QSAR methods. Tartu, 2015, 123 p.
144. **Olga Mazina.** Development and application of the biosensor assay for measurements of cyclic adenosine monophosphate in studies of G protein-coupled receptor signaling. Tartu, 2015, 116 p.
145. **Sandip Ashokrao Kadam.** Anion receptors: synthesis and accurate binding measurements. Tartu, 2015, 116 p.
146. **Indrek Tallo.** Synthesis and characterization of new micro-mesoporous carbide derived carbon materials for high energy and power density electrical double layer capacitors. Tartu, 2015, 148 p.
147. **Heiki Erikson.** Electrochemical reduction of oxygen on nanostructured palladium and gold catalysts. Tartu, 2015, 204 p.
148. **Erik Anderson.** *In situ* Scanning Tunnelling Microscopy studies of the interfacial structure between Bi(111) electrode and a room temperature ionic liquid. Tartu, 2015, 118 p.
149. **Girinath G. Pillai.** Computational Modelling of Diverse Chemical, Biochemical and Biomedical Properties. Tartu, 2015, 140 p.
150. **Piret Pikma.** Interfacial structure and adsorption of organic compounds at Cd(0001) and Sb(111) electrodes from ionic liquid and aqueous electrolytes: an *in situ* STM study. Tartu, 2015, 126 p.
151. **Ganesh babu Manoharan.** Combining chemical and genetic approaches for photoluminescence assays of protein kinases. Tartu, 2016, 126 p.
152. **Carolin Siimenson.** Electrochemical characterization of halide ion adsorption from liquid mixtures at Bi(111) and pyrolytic graphite electrode surface. Tartu, 2016, 110 p.
153. **Asko Laaniste.** Comparison and optimisation of novel mass spectrometry ionisation sources. Tartu, 2016, 156 p.
154. **Hanno Evard.** Estimating limit of detection for mass spectrometric analysis methods. Tartu, 2016, 224 p.
155. **Kadri Ligi.** Characterization and application of protein kinase-responsive organic probes with triplet-singlet energy transfer. Tartu, 2016, 122 p.
156. **Margarita Kagan.** Biosensing penicillins' residues in milk flows. Tartu, 2016, 130 p.
157. **Marie Kriisa.** Development of protein kinase-responsive photoluminescent probes and cellular regulators of protein phosphorylation. Tartu, 2016, 106 p.
158. **Mihkel Vestli.** Ultrasonic spray pyrolysis deposited electrolyte layers for intermediate temperature solid oxide fuel cells. Tartu, 2016, 156 p.
159. **Silver Sepp.** Influence of porosity of the carbide-derived carbon on the properties of the composite electrocatalysts and characteristics of polymer electrolyte fuel cells. Tartu, 2016, 137 p.
160. **Kristjan Haav.** Quantitative relative equilibrium constant measurements in supramolecular chemistry. Tartu, 2017, 158 p.

161. **Anu Teearu.** Development of MALDI-FT-ICR-MS methodology for the analysis of resinous materials. Tartu, 2017, 205 p.
162. **Taavi Ivan.** Bifunctional inhibitors and photoluminescent probes for studies on protein complexes. Tartu, 2017, 140 p.
163. **Maarja-Liisa Oldekop.** Characterization of amino acid derivatization reagents for LC-MS analysis. Tartu, 2017, 147 p.
164. **Kristel Jukk.** Electrochemical reduction of oxygen on platinum- and palladium-based nanocatalysts. Tartu, 2017, 250 p.
165. **Siim Kukk.** Kinetic aspects of interaction between dopamine transporter and *N*-substituted nortropine derivatives. Tartu, 2017, 107 p.
166. **Birgit Viira.** Design and modelling in early drug development in targeting HIV-1 reverse transcriptase and Malaria. Tartu, 2017, 172 p.
167. **Rait Kivi.** Allosteric in cAMP dependent protein kinase catalytic subunit. Tartu, 2017, 115 p.
168. **Agnes Heering.** Experimental realization and applications of the unified acidity scale. Tartu, 2017, 123 p.
169. **Delia Juronen.** Biosensing system for the rapid multiplex detection of mastitis-causing pathogens in milk. Tartu, 2018, 85 p.
170. **Hedi Rahnel.** ARC-inhibitors: from reliable biochemical assays to regulators of physiology of cells. Tartu, 2018, 176 p.
171. **Anton Ruzanov.** Computational investigation of the electrical double layer at metal–aqueous solution and metal–ionic liquid interfaces. Tartu, 2018, 129 p.
172. **Katrin Kestav.** Crystal Structure-Guided Development of Bisubstrate-Analogue Inhibitors of Mitotic Protein Kinase Haspin. Tartu, 2018, 166 p.
173. **Mihkel Ilisson.** Synthesis of novel heterocyclic hydrazine derivatives and their conjugates. Tartu, 2018, 101 p.
174. **Anni Allikalt.** Development of assay systems for studying ligand binding to dopamine receptors. Tartu, 2018, 160 p.
175. **Ove Oll.** Electrical double layer structure and energy storage characteristics of ionic liquid based capacitors. Tartu, 2018, 187 p.
176. **Rasmus Palm.** Carbon materials for energy storage applications. Tartu, 2018, 114 p.
177. **Jürgen Metsik.** Preparation and stability of poly(3,4-ethylenedioxythiophene) thin films for transparent electrode applications. Tartu, 2018, 111 p.
178. **Sofja Tšepelevitš.** Experimental studies and modeling of solute-solvent interactions. Tartu, 2018, 109 p.
179. **Märt Lõkov.** Basicity of some nitrogen, phosphorus and carbon bases in acetonitrile. Tartu, 2018, 104 p.
180. **Anton Mastitski.** Preparation of α -aza-amino acid precursors and related compounds by novel methods of reductive one-pot alkylation and direct alkylation. Tartu, 2018, 155 p.
181. **Jürgen Vahter.** Development of bisubstrate inhibitors for protein kinase CK2. Tartu, 2019, 186 p.

182. **Piia Liigand.** Expanding and improving methodology and applications of ionization efficiency measurements. Tartu, 2019, 189 p.
183. **Sigrid Selberg.** Synthesis and properties of lipophilic phosphazene-based indicator molecules. Tartu, 2019, 74 p.
184. **Jaanus Liigand.** Standard substance free quantification for LC/ESI/MS analysis based on the predicted ionization efficiencies. Tartu, 2019, 254 p.
185. **Marek Mooste.** Surface and electrochemical characterisation of aryl film and nanocomposite material modified carbon and metal-based electrodes. Tartu, 2019, 304 p.
186. **Mare Oja.** Experimental investigation and modelling of pH profiles for effective membrane permeability of drug substances. Tartu, 2019, 306 p.
187. **Sajid Hussain.** Electrochemical reduction of oxygen on supported Pt catalysts. Tartu, 2019, 220 p.
188. **Ronald Väli.** Glucose-derived hard carbon electrode materials for sodium-ion batteries. Tartu, 2019, 180 p.
189. **Ester Tee.** Analysis and development of selective synthesis methods of hierarchical micro- and mesoporous carbons. Tartu, 2019, 210 p.
190. **Martin Maide.** Influence of the microstructure and chemical composition of the fuel electrode on the electrochemical performance of reversible solid oxide fuel cell. Tartu, 2020, 144 p.
191. **Edith Viirlaid.** Biosensing Pesticides in Water Samples. Tartu, 2020, 102 p.
192. **Maike Käärrik.** Nanoporous carbon: the controlled nanostructure, and structure-property relationships. Tartu, 2020, 162 p.
193. **Artur Gornischeff.** Study of ionization efficiencies for derivatized compounds in LC/ESI/MS and their application for targeted analysis. Tartu, 2020, 124 p.
194. **Reet Link.** Ligand binding, allosteric modulation and constitutive activity of melanocortin-4 receptors. Tartu, 2020, 108 p.
195. **Pilleriin Peets.** Development of instrumental methods for the analysis of textile fibres and dyes. Tartu, 2020, 150 p.
196. **Larisa Ivanova.** Design of active compounds against neurodegenerative diseases. Tartu, 2020, 152 p.
197. **Meelis Härmas.** Impact of activated carbon microstructure and porosity on electrochemical performance of electrical double-layer capacitors. Tartu, 2020, 122 p.
198. **Ruta Hecht.** Novel Eluent Additives for LC-MS Based Bioanalytical Methods. Tartu, 2020, 202 p.
199. **Max Hecht.** Advances in the Development of a Point-of-Care Mass Spectrometer Test. Tartu, 2020, 168 p.
200. **Ida Rahu.** Bromine formation in inorganic bromide/nitrate mixtures and its application for oxidative aromatic bromination. Tartu, 2020, 116 p.
201. **Sander Ratso.** Electrocatalysis of oxygen reduction on non-precious metal catalysts. Tartu, 2020, 371 p.
202. **Astrid Darnell.** Computational design of anion receptors and evaluation of host-guest binding. Tartu, 2021, 150 p.

203. **Ove Korjus.** The development of ceramic fuel electrode for solid oxide cells. Tartu, 2021, 150 p.
204. **Merit Oss.** Ionization efficiency in electrospray ionization source and its relations to compounds' physico-chemical properties. Tartu, 2021, 124 p.
205. **Madis Lüsi.** Electroreduction of oxygen on nanostructured palladium catalysts. Tartu, 2021, 180 p.
206. **Eliise Tammekivi.** Derivatization and quantitative gas-chromatographic analysis of oils. Tartu, 2021, 122 p.
207. **Simona Selberg.** Development of Small-Molecule Regulators of Epi-transcriptomic Processes. Tartu, 2021, 122 p.
208. **Olivier Etebe Nonga.** Inhibitors and photoluminescent probes for in vitro studies on protein kinases PKA and PIM. Tartu, 2021, 189 p.
209. **Riinu Härmas.** The structure and H₂ diffusion in porous carbide-derived carbon particles. Tartu, 2022, 123 p.
210. **Maarja Paalo.** Synthesis and characterization of novel carbon electrodes for high power density electrochemical capacitors. Tartu, 2022, 144 p.